

6.7 GHz methanol maser survey toward GLIMPSE point sources and BGPS 1.1 mm dust clumps

Yan Sun^{1,2,3}, Ye Xu¹, Xi Chen⁴, Bo Zhang^{4,5}, Yuan-Wei Wu^{1,5}, Christian Henkel^{5,6}, Andreas Brunthaler⁵, Yoon Kyung Choi⁵, and Xing-Wu Zheng⁷

¹ Purple Mountain Observatory, Chinese Academy of Sciences, 210008 Nanjing, PR China
e-mail: yansun@pmo.ac.cn

² Graduate University of the Chinese Academy of Sciences, 19A Yuquan road, Shijingshan District, 100049 Beijing, PR China

³ Key Laboratory of Radio Astronomy, Chinese Academy of Sciences, Beijing 100049, PR China

⁴ Shanghai Astronomical Observatory, Chinese Academy of Sciences, 200030 Shanghai, PR China

⁵ Max-Planck-Institut für Radioastronomie, auf dem Hügel 69, 53121 Bonn, Germany

⁶ Astronomy Department, Faculty of Science, King Abdulaziz University, PO Box 80203, 21589 Jeddah, Saudi Arabia

⁷ School of Astronomy and Space Science, Nanjing University, 210093 Nanjing, PR China

Received 13 November 2013 / Accepted 24 January 2014

ABSTRACT

We present the results of a 6.7 GHz methanol maser survey from the Effelsberg 100 m radio telescope. A sample of 404 sources from the Bolocam Galactic Plane Survey (BGPS) 1.1 mm dust clump survey that met specific Galactic Legacy Infrared Mid-Plane Survey Extraordinaire (GLIMPSE) point-source color criteria was selected and 318 of these were observed. The new observations resulted in the detection of 29 methanol masers, including 12 new ones. Together with the additional 74 detections from the literature, this means that a total of 103 methanol masers are coincident with 1.1 mm dust clumps, yielding an overall detection rate of 26%. A comparison of the properties of a 1.1 mm dust clump and a 6.7 GHz methanol maser indicates that methanol masers with a higher flux density and/or luminosity are generally associated with more massive but less dense 1.1 mm dust clumps. The overall detection rate of 26% appears to vary as a function of the derived H₂ column density of the associated 1.1 mm dust clump. The methanol masers were primarily detected toward the brighter and more massive 1.1 mm dust clumps. A subsample of 194 sources that overlapped sources with observations of the 95 GHz methanol line was investigated in more detail for the properties of 1.1 mm dust clumps. The statistical analysis reveals that 1.1 mm dust clumps with both class I and II counterparts have much higher mean and median values of mass, column density, and flux density than those with only class I or II counterparts. Based on our much larger sample, we slightly revise the boundary defined previously for selecting BGPS sources associated with a class II methanol maser, wherein ~80% of expected class II methanol masers will be detected with a detection rate in the range of 40–50%.

Key words. masers – stars: formation – ISM: molecules – radio lines: ISM – infrared: ISM

1. Introduction

Masers are one of the most readily observed signposts of star formation. Methanol masers represent the most common type of masers because they are seen in a variety of lines and because they are relatively intense, particularly those at 6.7 and 12.2 GHz. Different maser lines are tracing quite a variety of physical environments, and thus they are able to trace different evolutionary phases of star formation (Ellingsen 2007; Breen et al. 2010). In addition, masers are not only powerful probes of the kinematics around the star formation regions (Moscadelli et al. 2010), but also excellent tools for determining their accurate distances by measuring their trigonometric parallaxes (Reid et al. 2009).

Methanol masers have been empirically divided into two groups: class I and class II. The former species is common in both low- and high-mass star-forming regions (Kalenskii et al. 2006, 2010). Unlike class I methanol masers, class II methanol masers are exclusively associated with massive star-forming regions (e.g., Walsh et al. 2001; Minier et al. 2003), and have

received the most attention. During the past decade, extensive maser surveys have been performed for class II methanol masers (especially at 6.7 GHz), which resulted in an overall detection of ~900 class II maser sources in the Galaxy (e.g., Pestalozzi et al. 2005; Ellingsen 2007; Pandian et al. 2007; Xu et al. 2008, 2009; Green et al. 2009, 2010, 2012; Fontani et al. 2010; and Caswell et al. 2010, 2011). Nevertheless, the nature of methanol masers is not yet fully understood. Therefore, more searches for class II methanol masers are essential.

Most of the previously conducted methanol surveys have typically targeted regions selected on the basis of IRAS colors (e.g., Szymczak et al. 2000). From the Galactic Legacy Infrared Mid-Plane Survey Extraordinaire (GLIMPSE) point-source colors, Ellingsen (2006) developed new criteria for targeting class II methanol maser searches. He found that 80% of class II methanol masers were detected toward GLIMPSE point sources, which have a brightness lower than 10 mag in the 8.0 μ m band (written as $[8.0] < 10$) and a color higher than 1.3 mag when comparing the 3.6 μ m and 4.5 μ m bands ($[3.6] - [4.5] > 1.3$). The subsequent observations of 113

known 6.7 GHz methanol masers associated with 1.1 mm dust continuum emission also resulted in a very high detection rate of 60% for 12.2 GHz methanol masers (Breen et al. 2010).

A recently released catalog of the Bolocam Galactic Plane Survey (BGPS; Rosolowsky et al. 2010; Aguirre et al. 2011), containing approximately 84 000 dust clumps detected in the 1.1 mm continuum, may be a useful supplement to the GLIMPSE catalog in constructing a reliable and efficiently targeted sample for a class II methanol maser survey. Using the Purple Mountain Observatory (PMO) 13.7 m radio telescope, Chen et al. (2012, hereafter C2012) have undertaken a 95 GHz class I methanol maser survey of a sample of 214 sources that come from a subsample of GLIMPSE point sources with associated BGPS 1.1 mm dust clumps. Class I methanol maser emissions were detected in 63 sources, corresponding to a detection rate of 29% for their survey.

Here, we report on the results of a 6.7 GHz methanol maser survey conducted with the Effelsberg 100 m radio telescope targeted at a similar but much larger sample, which overlaps both the BGPS and GLIMPSE sources. First, the sample selection and observations are described in Sect. 2, and in Sect. 3 the detections of class II methanol masers are presented. Next, in Sect. 4 the physical properties of the clumps and their associated masers are listed along with a statistical analysis. In Sect. 5 a summary of the results is given.

2. Source selection and observations

2.1. Target selection

The released catalogs of GLIMPSE (version 2.0) and BGPS (version 1.0.1) were used to construct a target sample for our 6.7 GHz class II methanol maser survey.

A sample of 404 GLIMPSE point sources with 1.1 mm dust clump associations was selected by applying the following criteria: (1) the GLIMPSE point sources have $[3.6] - [4.5] > 1.3$, $[3.6] - [5.8] > 2.5$, $[3.6] - [8.0] > 2.5$ and an 8.0 μm magnitude lower than 10; (2) the GLIMPSE point sources are associated with the 1.1 mm dust clumps within the full width at half-maximum (FWHM) of BGPS $\sim 30''$; (3) the declination of each source must be higher than -25° ; (4) the separation of each source must be larger than the FWHM of the Effelsberg 100 m $\sim 40''$ at 1.3 cm band (because we will search 22 GHz water maser emission in the next step in the same sample), otherwise the strongest source was adopted. The position of the 1.1 mm BGPS emission peak was adopted as the target position (listed in Table B.1). Our sample significantly overlaps that of C2012, which is marked *C* in Table B.1 (194 sources). Both (1) and (2) ensure that our sample is most likely undergoing a star-forming process and therefore a high detection rate of maser emission is expected. Due to observing time constraints, 13 sources lacked valid data; they are marked † in Table B.1. This reduced our sample size to 391 sources.

2.2. Existing methanol maser detections

We cross-correlated our sample with catalogs and large surveys of class II methanol masers. The catalog of the methanol multi-beam (MMB) survey (Caswell et al. 2010, 2011; Green et al. 2010, 2012) was used along with the recent work of Szymczak et al. (2012). The MMB survey provides a complete census of masers located in the 186° to 20° longitude region. The catalog of Szymczak et al. (2012) consists of 289 masers located in the 8° to 90° longitude region. The positions of subarcsecond accuracy are given for most of the objects. We considered a

methanol maser to be associated with a BGPS dust clump when its position fell within the radius of a BGPS clump. A radius of $130''$, the largest radius of sources found in this sample, was adopted for sources with no radius given. This simple radius search identified 84 potential associations, most of which were excluded from this observation (marked with * in Table B.1), and only eleven remained for cross-checking.

The properties of all associations are listed in Table B.2. The offset between the peak of the BGPS dust emission and the matched maser source is also listed in Table B.2. Note that the coordinates of masers given in Table B.2 are derived mainly from high angular resolution studies (e.g., Caswell 2009; Caswell et al. 2010; Green et al. 2010; Pandian et al. 2011).

2.3. Effelsberg observations

Within the available observing time, a total of 318 targets were observed. The observations were made using the Effelsberg 100 m telescope in October and November 2011. The rest frequency adopted for the 5_1-6_0 A^+ transition was 6668.519 MHz, corresponding to a FWHM beam of $\sim 2'$. The spectrometer was configured to have a 20 MHz bandwidth with 16 384 spectral channels yielding a spectral resolution of 0.055 km s^{-1} and a velocity coverage of 895 km s^{-1} . The system temperature was typically around 20 K during our observations. The flux density scale was determined by observing NGC 7027 and 3C 286 (Ott et al. 1984). The flux calibration uncertainty is estimated to be on the order of $\sim 10\%$. The on-source time for each position was about 2 min, and once the two available orthogonal polarizations were averaged, they yielded a typical rms noise of ~ 0.4 Jy after smoothing to a velocity resolution of 0.11 km s^{-1} to reduce the noise level in individual channels. When a source was detected, the integration time was increased to between 6 and 10 min. depending on its intensity. All spectral data were reduced and analyzed with the GILDAS/CLASS¹ package.

3. Results

3.1. General overview

Our survey resulted in the detection of 29 6.7 GHz methanol masers at or above the 3σ limit and one highly variable maser at about 2σ out of a total of 318 sources, which corresponds to a detection rate of 9%. The sensitivity achieved and the spectra with a resolution of 0.11 km s^{-1} detected in this survey are shown in Fig. A.1. The peak flux densities range from 0.5 to 60.3 Jy. The re-observations of the eleven sources with prior maser detections also show apparent maser detections in our new observations, with one exception. The exception is the highly variable source G06.189-0.358, which had a peak flux density of 229 Jy (Green et al. 2010) and was only marginally detected at 0.5 Jy (about 2σ) in our survey. After close inspection, we found that seven maser detections may have suffered from confusion due to strong nearby sources, marked on the individual spectra in Fig. A.1. Therefore, our survey detected 12 new sources subject to high-resolution confirmation and their details can be found in the comments. The new maser detections and detections that may merely represent sidelobe emission from nearby stronger masers are marked * and \triangleleft in Table 1, respectively. Since we did not attempt to determine the positions of the methanol masers using a five-point grid observation, the positions quoted in Table B.1 may have an error as high as $\sim 1'$.

¹ <http://www.iram.fr/IRAMFR/GILDAS>

Table 1. Related parameters of the class II methanol masers observed with the Effelsberg 100 m radio telescope.

PID	Maser	Offset	Distance	6.7 GHz CH ₃ OH							BGPS source			
				V_{start}	V_{end}	V_p	S_p	S_{int}	Luminosity	ref.	M	$n(\text{H}_2)$	$N(\text{H}_2)$	
(1)	(2)	(3)	(kpc)	km s ⁻¹	km s ⁻¹	km s ⁻¹	(Jy)	(Jy km s ⁻¹)	(10 ⁻⁷ L _⊙)	(11)	(M _⊙)	(10 ³ cm ⁻³)	(10 ²² cm ⁻²)	
1175	06.189-0.358	7	5.1 ^G	-37.5	-27.1	-30.2	0.5(0.25)		0.8	6.5	0, 2	2420	5.8	2.8
1682	12.199-0.033	7	12.0 ^G	48.2	57.3	49.3	14.6(0.17)		22.3	1004.9	0, 2	5963	0.8	1.1
1796 [‡]	12.909-0.260	175	3.6 ^S	38.6	40.6	39.8	2.3(0.13)		2.4	9.9	0	364	–	–
1809	12.904-0.031	4	4.6 ^S	58.2	60.4	58.8	60.3(0.24)		44.4	293.5	0, 2	1509	2.0	1.2
2246	16.112-0.303	12	3.0 ^G	34.1	35.1	34.5	2.2(0.11)		1.0	2.8	0, 2	69	1.6	0.4
2467	18.888-0.475	3	3.8 ^G	52.9	57.9	56.5	6.3(0.13)		8.2	37.2	0, 2	2853	1.8	1.4
2579	19.496+0.115	14	9.8 ^G	120.7	121.8	121.1	4.8(0.14)		2.2	66.7	0, 2	2350	0.3	0.4
2619	19.755-0.128	4	9.9 ^G	115.9	123.4	123.0	2.2(0.08)		1.7	53.3	0, 2	5386	0.5	0.7
2994 [‡]	23.010-00.411	293	4.2 ^N	72.8	76.6	74.9	1.2(0.09)		1.9	10.6	0	762	0.8	0.5
3081 [‡]	23.437-0.184	135	5.4 ^S	96.3	108.1	97.7	2.4(0.11)		6.9	62.9	0	1189	1.3	0.8
3383*	24.63+00.16	–	3.5 ^S	113.8	115.6	114.4	1.3(0.09)		0.7	2.6	0	497	3.2	1.1
3474*	25.23+00.29	–	3.2 ^S	41.2	42.3	41.8	0.7(0.11)		0.2	0.7	0	458	6.1	1.7
3591*	25.81-00.04	–	5.1 ^S	97.1	98.1	97.4	1.3(0.20)		0.5	3.8	0	1344	1.7	1.0
3616*	25.92-00.14	–	5.6 ^N	111.4	115.6	113.9	1.4(0.10)		1.2	12.1	0	347	0.8	0.4
3690 [‡]	26.53-0.27	185	5.8 ^S	102.1	110.5	107.1	1.0(0.09)		1.9	20.3	0	2307	1.1	0.9
3807*	27.56+00.08	–	4.8 ^S	78.2	88.5	87.2	2.5(0.11)		1.9	13.7	0	1622	3.3	1.7
3917*	28.22+00.36	–	3.0 ^N	48.4	51.5	50.3	7.7(0.15)		6.4	17.7	0	118	0.8	0.3
4398*	30.42-00.23	–	5.9 ^S	102.4	105.1	103.0	14.1(0.14)		6.6	72.6	0	5435	1.4	1.4
4403	30.42+0.46	9	1.3 ^S	4.5	9.2	6.4	0.7(0.06)		1.8	0.9	0, 3	76	2.2	0.5
4636*	30.98+00.22	–	6.2 ^S	110.0	111.8	110.9	1.0(0.10)		0.5	6.0	0	2032	0.4	0.4
4673*	31.08+00.46	–	2.2 ^S	24.7	27.6	25.7	2.1(0.10)		2.1	3.2	0	209	2.3	0.7
4701*	31.18-00.15	–	2.7 ^N	42.6	50.1	46.2	2.7(0.17)		3.8	8.8	0	266	1.2	0.5
5050 [‡]	32.745-0.076	118	12.0 ^G	29.4	39.8	38.5	8.9(0.26)		19.4	872.5	0	1693	0.2	0.2
5342*	34.26-00.21	–	3.1 ^N	49.5	55.4	54.6	9.0(0.13)		7.3	21.7	0	195	1.3	0.5
6323 [‡]	49.490-0.388	823	5.5 ^S	58.6	60.3	59.3	0.7(0.06)		0.4	3.7	0	3669	5.7	3.2
6346 [‡]	49.490-0.388	313	5.5 ^S	57.6	60.4	59.3	5.1(0.17)		3.9	36.4	0	2171	2.9	1.7
6414	53.142+0.071	10	1.6 ^G	23.9	25.4	24.7	1.1(0.21)		0.6	0.5	0, 3	287	12.8	2.4
6433	53.618+0.036	6	8.7 ^G	18.3	19.7	18.9	6.0(0.11)		2.7	64.4	0, 3	2876	2.2	1.6
6470*	56.96-00.23	–	3.5 ^S	29.3	30.6	29.8	1.1(0.06)		0.4	1.6	0	151	7.6	1.4
6479	59.63-0.19	23	3.5 ^S	28.4	31.2	29.6	0.9(0.10)		0.5	1.9	0, 3	1132	15.2	4.2

Notes. Note that the 2σ detection is included. Detailed comments and references on the sources are also given in Sect. 3.2. Column (1): PID number of BGPS source, all new detections in this survey are marked by *, detections that might be a side-lobe of a nearby stronger maser are marked by ‡. Column (2): Galactic coordinates of the associated masers. Column (3): angular offset between the peak of the 1.1 mm dust emission and the maser position. Column (4): adopted distance for sources overlapped with Green & McClure-Griffiths (2011), Dunham et al. (2011) or Schlingman et al. (2011); we preferentially adopted the distances estimated from their work, which are marked by *G*, *D* and *S*, otherwise we assumed the near kinematic distance computed from the peak velocity of the 6.7 GHz masers, which are marked *N*. Columns (5)–(10): radial velocity range, radial velocity of the peak emission, peak flux density (the values in brackets present the rms levels of each detection with a velocity resolution of 0.11 km s⁻¹), integrated flux density and luminosity of 6.7 GHz methanol maser. Column (11): references for maser information. 0 this survey, 1 Caswell et al. (2010), 2 Green et al. (2010), 3 Szymczak et al. (2012). Columns (12)–(14): derived gas mass and averaged H₂ volume and column densities of the BGPS source, respectively.

Combining an additional 74 associations (including the variable source detected at 2σ by us) taken directly from the literature (e.g. Caswell et al. 2010; Green et al. 2010; Szymczak et al. 2012) with the 29 detections from our observations, a total of 103 6.7 GHz methanol masers are associated with 1.1 mm dust clumps for the entire sample, yielding an overall detection rate of 26%.

The distances in Table B.2 and Table 1 are primarily taken from the literature, particularly from Green & McClure-Griffiths (2011), who directly resolved the distance ambiguity by HI self-absorption (HISA) from the Southern Galactic Plane Survey (SGPS). We have marked these sources with a *G*. Those marked *S* and *D* come from Schlingman et al. (2011) and Dunham et al. (2011), who estimated the distances from molecular line observations (e.g., NH₃, HCO⁺ and N₂H⁺). Distances to a few sources without available data were computed from the peak velocity of 6.7 GHz masers by using the Galactic rotation

model of Reid et al. (2009), assuming $R_{\odot} = 8.4$ kpc and $\Theta_0 = 254$ km s⁻¹. Because most parallax distances from VLBI observations are close to the near kinematic distances (e.g., Xu et al. 2009), a near kinematic solution was assumed for these sources. However, because the Galactic rotation model cannot provide a reliable distance for the source PID 1508, we adopted distances from C2012 (marked *C*).

3.2. Comments on individual BGPS sources

Below we summarize each BGPS source in more detail. This includes 11 sources that are associated with previously known maser sources (note that the 2σ detection is included), 7 sources that might be confused with known maser sources, and 12 new maser sources (P3383, 3474, 3591, 3616, 3807, 3917, 4398, 4636, 4673, 4701, 5342, and 6470). We refer here to the previous subsection, from where the numbers have been taken.

P1175 G006.191-00.359. This source was only marginally detected at 0.5 Jy (about 2σ) in our survey. The known maser source G06.189-0.358 (offset by $7''$) was discovered by Green et al. (2010) with a 6.7 GHz methanol peak flux density of 229 Jy (with data taken in 2007). The variability compared with the literature is remarkable on a time scale of 3.5 years, which is comparable with the most extreme variable example of G351.42+0.64 reported by Goedhart et al. (2004). In the latter case the peak flux density increased from below the detection limit of 1.5 to 250 Jy in two months. Future regular monitoring of these sources is necessary to interpret the extreme variability.

P1682 G012.201-00.034. The position of the known source G12.199-0.033 was determined with ATCA in 1997 (Caswell 2009) by finding a feature with a peak flux density of 12.5 Jy at 49.3 km s^{-1} . Green et al. (2010) detected a brighter feature with a flux density of 13.7 Jy at the same velocity with the Parkes radio telescope.

P1796 G012.861-00.272. There are two blended features between 38.6 and 40.6 km s^{-1} that may be a side-lobe response of the previously known source G12.909-0.260 (offset by $175''$) with a peak flux density of ~ 300 Jy (Menten 1991; Caswell 2009; Green et al. 2010).

P1809 G012.905-00.030. This source shows a double-peaked structure, one at 58.8 km s^{-1} of 60.3 Jy and another at 59.5 km s^{-1} of 29.3 Jy. However, Green et al. (2010) found the strongest feature of the known source G12.904-0.031 at 59.1 km s^{-1} decreased from ~ 40 Jy in 2007 to ~ 20 Jy in 2008. This source is associated with an extended green object (EGO; Cyganowski et al. 2008). Recent studies suggest that EGOS are young stellar objects with active outflows (Cyganowski et al. 2009; Lee et al. 2012; Chen et al. 2013).

P2246 G016.114-00.301. Our peak flux density of 2.2 Jy is virtually the same as that of the known source G16.112-0.303, which was reported by Green et al. (2010) with data taken in 2008.

P2467 G018.888-00.475. This source is associated with an EGO. The known source G18.888-0.475 was also recently detected by Cyganowski et al. (2009) and Green et al. (2010). There are at least five features between 52.8 and 57.9 km s^{-1} . The brightest feature has remained relatively constant at ~ 6 Jy, but one weak feature at 55.8 km s^{-1} has increased from ~ 1.8 Jy (Green et al. 2010) to 3.2 Jy (our new data).

P2579 G019.498+00.119. The known source G19.496+0.115 was previously detected by Caswell (2009) and Green et al. (2010). Its position was obtained by Caswell (2009) with the ATCA.

P2619 G019.756-00.129. There are two features separated by $\sim 7 \text{ km s}^{-1}$ with a peak flux density of 3.63 Jy in the known source G19.755-0.128 (taken with the Parkes radio telescope), while our value is 2.3 Jy. This source is not only fully within the Parkes, but also within the Effelsberg beam size. The major feature may be variable, whereas the weaker feature of ~ 2 Jy at 116.3 km s^{-1} does not appear to be variable.

P2994 G023.090-00.394. This source was observed as a single feature at 74.9 km s^{-1} with a peak flux density of 1.2 Jy. The known source G23.010-00.411 (offset by $293''$) had a peak flux density of ~ 500 Jy at 74.7 km s^{-1} (Menten 1991; Xu et al. 2009; Szymczak et al. 2012). The aligned spectra imply that the nearby brighter source may be responsible for our current detection.

P3081 G023.462-00.156. There are at least two blended peaks between 95 and 100 km s^{-1} and three features between 101 and 109 km s^{-1} . All of these features may partially be a side-lobe

response of known sources, G23.437-0.184 and G23.440-0.182 (Menten 1991; Caswell 2009; Szymczak et al. 2012).

P3383 G024.632+00.155. IRAS 18331-0717 separated by $281''$ from this source was not detected in the 6.7 GHz methanol line with a limit of 0.43 Jy (1σ) and a velocity resolution of 0.04 km s^{-1} (Szymczak et al. 2000). However, a clear feature of 1.3 Jy at 114.4 km s^{-1} is a new detection. This source was also detected in 95 GHz class I methanol (Chen et al. 2012) and is associated with an EGO listed as G024.63+0.15 (Cyganowski et al. 2008).

P3474 G025.227+00.289. Szymczak et al. (2000) did not detect the 6.7 GHz methanol emission with a limit of 0.43 Jy (1σ) and a velocity resolution of 0.04 km s^{-1} , while a weak feature of 0.7 Jy at 41.8 km s^{-1} is newly detected in our observations.

P3591 G025.805-00.041. This new source primarily shows a single 6.7 GHz methanol feature at 97.4 km s^{-1} . Except for cold dust emission from the BGPS, no other observation has been reported in this region. IRAS 18358-0623, which is separated by $\sim 20''$, may be associated with it.

P3616 G025.920-00.139. Although spatially close to molecular cloud SRBY 128 (Solomon et al. 1987), the peak velocity of this new maser source at 113.9 km s^{-1} does not match the radial velocity of SRBY 128 at 104.8 km s^{-1} from $^{13}\text{CO}(1-0)$ emission (Heyer et al. 2009).

P3690 G026.562-00.303. G26.53-0.27 (IRAS 18380-0548), separated by $\sim 185''$, was not detected through 6.7 GHz methanol emission with a limit of 0.62 Jy (1σ) and a velocity resolution of 0.04 km s^{-1} (Szymczak et al. 2000), but was found to contain multiple features spanning from 102 to 115.3 km s^{-1} with a peak flux density of 5.5 Jy by Szymczak et al. (2012). Our detection of multiple features spanning from 102.1 to 110.5 km s^{-1} with a peak flux density of 1 Jy is probably a side-lobe response to the known source.

P3807 G027.562+00.080. A single feature ranging from 86.0 to 88.5 km s^{-1} dominates the emission of this new maser source in addition to a weak spectral feature that appears to be at $\sim 80 \text{ km s}^{-1}$.

P3917 G028.222+00.358. This new source contains three 6.7 GHz methanol features between 48.4 and 51.5 km s^{-1} . IRAS 18389-0404, separated by $\sim 18''$, may be associated with it.

P4398 G030.419-00.232. This source is the brightest ($S_p \sim 14.1$ Jy) new source detection of this survey. It is associated with an EGO, listed as G030.42-0.23 (Cyganowski et al. 2008). IRAS 18450-0224, separated by $\sim 21''$, may also be part of it.

P4403 G030.423+00.466. The known source G30.42+0.46 (IRAS 18426-0204), separated by $\sim 9''$, was not detected by 6.7 GHz methanol emission with 0.55 Jy limits (1σ , Szymczak et al. 2000). But it was first detected by Sridharan et al. (2002) with a peak flux density of 1.3 Jy and was detected again by Szymczak et al. (2012) with virtually the same flux density. In our new observation a peak flux density of 0.7 Jy at 6.4 km s^{-1} was obtained.

P4636 G030.980+00.215. This new source has a single narrow feature near 110.9 km s^{-1} with a peak flux density of 1.0 Jy. IRAS 18443-0141, separated by $\sim 110''$, may be associated with it.

P4673 G031.077+00.459. This new source contains two main 6.7 GHz methanol features, one with a peak flux density of 2.1 Jy at $\sim 25.7 \text{ km s}^{-1}$ and another with a peak flux density of 1.4 Jy at $\sim 26.5 \text{ km s}^{-1}$. G031.0494+00.4698, an HII region separated by $\sim 100''$, may be associated with it (Urquhart et al. 2009).

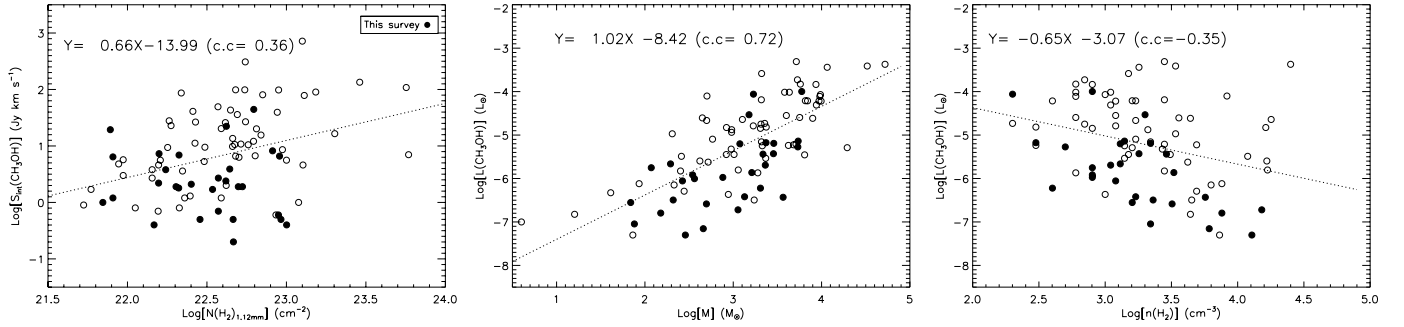


Fig. 1. Correlations between 6.7 GHz integrated flux density and beam-averaged H₂ column density (*left*), between 6.7 GHz luminosity and mass (*middle*), and between 6.7 GHz luminosity and H₂ volume density (*right*) of the associated 1.1 mm BGPS sources in the log-log plot. The dotted line in each panel represents the least-squares fit result to all data points. The correlation coefficient is also marked in each plot. Properties of the 6.7 GHz methanol masers are based on both this current survey and the literature (e.g., Caswell et al. 2010; Green et al. 2010; Szymczak et al. 2012), which are indicated by filled and open circles, respectively.

P4701 G031.182-00.145. The spectrum of this new source contains several blended features spanning from 42.6 to 50.1 km s⁻¹. An IRAS source 18461-0142 and an HII region, separated by ~80'' may be associated with it (Wood & Churchwell 1989; Becker et al. 1994).

P5050 G032.773-00.059. There are at least four features between 29.4 to 39.8 km s⁻¹ with a peak flux density of 8.9 Jy at 38.5 km s⁻¹. Toward G32.745-0.076 (IRAS 18487-0015), separated by ~118'', methanol emission was first found by Menten (1991) with a peak flux density of 46 Jy at ~38 km s⁻¹. A similar value was reported by Caswell et al. (1995) and Szymczak et al. (2000, 2012). The aligned spectra suggest that our detection represents the sidelobe response from a nearby brighter source.

P5342 G034.264-00.210. There are three features in this new source, with a peak emission of 9.0 Jy at 54.6 km s⁻¹. IRAS 18520+0101, separated by ~19'', may be associated with it. Apart from BGPS, no other research has been reported in this region.

P6323 G049.267-00.338 and P6346 G049.405-00.370. The two centers are separated by 513'', and shown on two aligned spectra in Fig. A.1. Prior knowledge about the known strong maser source G49.490-0.388 (offsets by 823'' and 313'', respectively) may lead to our observations. These sources are associated with the well-known complex W51. G049.267-00.338 is associated with an EGO (Cyganowski et al. 2008) as well as with a 95 GHz class I methanol maser (Chen et al. 2012).

P6414 G053.142+00.068 and P6433 G053.616+00.036. Two nearby known sources G53.142+0.071 (IRAS 19270+1750) and G53.618+0.036 (IRAS 19282+181) had peak flux densities of 1.9 Jy at 23.8 km s⁻¹ and 6.3 Jy at 18.7 km s⁻¹ when first detected by Szymczak et al. (2000). Recently, Szymczak et al. (2012) reported a flux density of 2.6 Jy at 23.8 km s⁻¹ and 7.9 Jy at 18.9 km s⁻¹. In our observation, the first source varied with a marginal detection of 0.6 Jy at 23.8 (fading by a factor of 0.25), while showing a peak flux density of 1.1 Jy at 24.7 km s⁻¹. The second source shows a peak flux density of 6.0 Jy at 18.9 km s⁻¹.

P6470 G056.962-00.234. This new source displays a narrow weak feature of 1.1 Jy. IRAS 19360+2101, separated by ~30'', may be associated with it.

P6479 G059.639-00.189. The spectrum is aligned with the velocity of the known maser G59.63-0.19 and separated by 23'' with a peak flux density of 3.3 Jy at 9.5 km s⁻¹ (Szymczak et al. 2012).

4. Discussion

4.1. Characteristics of the 6.7 GHz class II methanol masers

For better comparison, the methods used by C2012 were adopted to estimate the properties summarized in Tables B.1, B.2, and Table 1, including luminosity, beam-averaged H₂ column density, H₂ number density and mass. A log-log plot of the beam-averaged H₂ column density versus the integrated intensity of the 6.7 GHz methanol masers is shown in the left panel of Fig. 1. In addition, the log-log plots for the luminosity of the 6.7 GHz methanol masers as a function of the derived gas mass (middle panel) and H₂ volume density (right panel) of the associated 1.1 mm BGPS source are also shown in Fig. 1. The results of a least-squares fit and the correlation coefficients are marked in each plot. The luminosity and flux of the 6.7 GHz methanol masers increase with the mass and column density of the associated dust clumps, as is evident in the left and middle panels of Fig. 1. The more luminous 6.7 GHz methanol masers are associated with less dense 1.1 dust clumps and can be seen in the right panel of Fig. 1, with a slope of -0.65 and a correlation coefficient of 0.35.

Similar trends have been revealed by Breen et al. (2010) with a sample of ~110 6.7 GHz methanol masers, which does not significantly overlap with our sample (about 10%). To explain these trends, Breen et al. (2010) proposed an evolutionary scenario, assuming that the methanol sources increase in luminosity as they evolve. This hypothesis has also been confirmed by their subsequent publication (Breen et al. 2011). Similarly, Wu et al. (2010) revealed that the lower luminosity 6.7 GHz methanol masers are associated with smaller ammonia line widths and therefore they correspond to the younger sources, which also agrees with the findings of Breen et al. (2010, 2011).

In comparison with the results of Breen et al. (2010), our data points show a relatively larger scatter. Nevertheless, our results might still support their hypothesis. As previously noted, properties of most methanol masers were extracted from the literature, referring to different telescopes and epochs. Therefore, the bias introduced by time variability and calibration uncertainties among different instruments may largely account for the scatter. Another possible explanation are false associations caused by the positional inaccuracies. In addition, for the new masers, the flux uncertainty introduced by relatively poor positional accuracy also contributes to the scatter. In the middle and right panels, bias introduced by inaccuracy of distances should be taken into account as well.

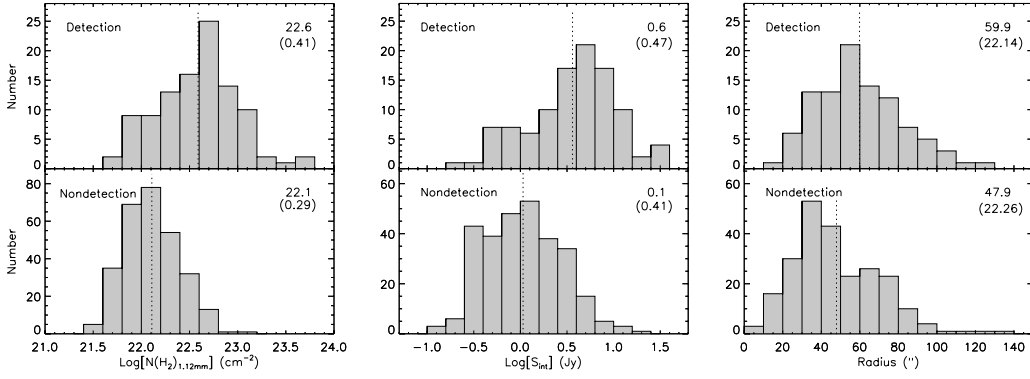


Fig. 2. Distributions of beam-averaged H₂ column density (*left*), 1.1 mm integrated flux density (*middle*), and angular radius (*right*) of the BGPS sources for the two groups with and without 6.7 GHz class II methanol maser detections. Together with the standard deviation, the mean value is marked and indicated by a dotted line in each plot.

Table 2. Statistical parameters for sources with and without associated 6.7 GHz class II methanol masers for the entire sample.

Property	Group	Mean	Standard deviation	Minimum	Median	Maximum
log[N _{H₂} ^{beam}] (cm ⁻²)	class II	22.6	0.41	21.7	22.6	23.8
	no class II	22.1	0.29	21.4	22.1	23.2
log[S _{int}] (Jy)	class II	0.6	0.47	-0.7	0.6	1.5
	no class II	0.1	0.41	-1.0	0.0	1.3
Radius (^{''})	class II	59.9	22.14	19.5	58.1	120.8
	no class II	47.9	22.26	5.1	43.9	133.8

4.2. Statistical analysis of sources with and without associated 6.7 GHz class II methanol masers

Chen et al. (2011, 2012) revealed that there are no clear differences in the mid-IR colors between sources with and without associated class I methanol masers. However, the properties of masers (including water masers, class I and II methanol masers) heavily depend on the properties of the associated dust clumps (e.g., Breen et al. 2007, 2010; Breen & Ellingsen 2011; Chen et al. 2011, 2012). To further investigate whether there are any differences in properties of mid-IR and/or 1.1 mm dust clumps with and without associated class II methanol masers, a statistical analysis was performed following the methods of C2012 and Breen et al. (2007).

The dust clumps were split into two groups depending on either the presence or absence of class II methanol masers. Because we lack distance measurements for the latter group, the intrinsic physical parameters such as mass and source size in pc are not discussed in this section. Note that the beam-averaged H₂ column density was directly derived from the $S_{40''}$ (1.1 mm flux density within an aperture with a diameter of 40^{''}), and therefore the $S_{40''}$ was excluded from the following statistical analysis.

Figure 2 shows the distributions of the beam-averaged H₂ column density (left panel), integrated flux density (middle panel), and angular radius (right panel), plotted as histograms for the two groups. Table 2 gives a summary of the basic statistical parameters, including the mean and median values and the standard deviations. We found that sources with associated 6.7 GHz class II methanol masers are more likely to have a higher column density, flux density, and radius than those without. The mean logarithmic value of column density of BGPS sources with class II methanol maser associations is 22.6 [cm⁻²], while it is 22.1 [cm⁻²] for those without. This result is expected because flux densities of BGPS sources will also fall off with distance (like methanol masers). The mean logarithmic value of the

integrated flux density of BGPS sources with class II methanol maser associations is 0.6 [Jy], while it is 0.1 [Jy] for those without. A certain degree of discrepancy in column density and flux density does exist between the two groups with a difference of approximately two standard deviations. However, the difference in radius is less statistically significant, with a mean value of ~50^{''} for both groups (a difference of less than one standard deviation). The mean values are marked in each corresponding panel of Fig. 2. The discovered trends are consistent with the results of C2012. Given the smaller overlap in the range of the beam-averaged column density for the two groups, as in C2012, we argue that the beam-averaged H₂ column density might provide a better criterion for identifying possible BGPS sources with associated class II methanol masers.

In contrast, the color-color diagram of our sample in Fig. 3 shows that there is no significant difference in the nature of the associated GLIMPSE point sources between the two groups (indicated by solid and open circles), consistent with previous similar studies (e.g. Chen et al. 2011, 2012). Just as for the class I methanol masers in C2012, the detection rate of class II methanol masers is not closely related to the mid-IR property, which therefore cannot provide the most efficient criterion. On the other hand, one Effelsberg beam (~2['] at 6.7 GHz) would contain a number of GLIMPSE point sources, and in the present observations with this resolution we cannot distinguish which one is the true association. Our assumption that the GLIMPSE point source, which meets the mid-IR color criteria, is associated with the maser inevitably introduces false associations in some cases. Therefore we do not discuss the mid-IR property here in more detail.

4.2.1. Binomially generalized linear model

A binomially generalized linear model (GLM; McCullagh & Nelder 1989) was also fitted to the maser presence/absence

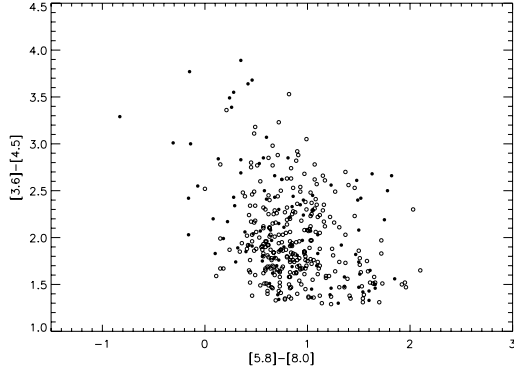


Fig. 3. Color-color diagram constructed from GLIMPSE point-source catalogs. Filled and open circles represent the sources with and without class II methanol maser detections, respectively.

Table 3. Analysis of deviance table for all possible single-term binomial models, including the AIC, associated likelihood ratio statistic and p -value.

Predictor	AIC	Deviance	LRT	p -value
none	403	401		
radius	386	382	18.6	1.6e-05
S_{int}	326	322	78.3	<2.2e-16
N_{H_2}	297	293	108.1	<2.2e-16

Notes. The p -value tests the hypothesis that the model provides no better fit than the null model, which consists of only an intercept; 1.1 mm dust clumps with and without 6.7 GHz class II methanol masers.

using 1.1 mm BGPS properties, similar to the method used by Breen et al. (2007, 2010) and Breen & Ellingsen (2011). For a more detailed description of this analysis method see Breen et al. (2007). The probability of finding a maser in the i th clump, p_i , can be predicted in terms of the clump properties $x_{1i} x_{2i} x_{3i} \dots x_{mi}$,

$$y_i \sim \text{Bin}(1, p_i)$$

$$\log \frac{p_i}{1 - p_i} = \beta_0 + \beta_1 x_{1i} + \beta_2 x_{2i} + \dots + \beta_m x_{mi},$$

where y_i is the maser presence or absence in the i th clump and $\beta_0, \beta_1, \beta_2 \dots \beta_m$ are the regression coefficients.

First, a single-term binomial model was tested on each property and compared by analyzing the deviance to the null model, which consists of only an intercept to investigate whether individually they might give an indication for the probability of finding an associated methanol maser. For each of the 332 dust clumps listed in Table B.1 with available radius, the considered clump properties were angular radius, integrated flux density (S_{int}) in Jy, and beam-averaged H_2 column density (N_{H_2} 10^{22} cm^{-3}). Then, the Akaike Information Criteria (AIC; Burnham & Anderson 2002) were used to select the most parsimonious model. P -values of less than 0.05 were considered to be statistically significant in the following analysis. All of the possible single-term binomial models are summarized in Table 3. The results reveal that any one of these dust clump properties can give an indication of the probability of methanol masers. The most simple model with the greatest predictive power of maser presence involves only N_{H_2} . The estimated regression relation can be expressed as

$$\log \frac{p_i}{1 - p_i} = -2.66938 + 0.6088 x_{N_{\text{H}_2}}, \quad (1)$$

Table 4. Estimated parameters for the binomial model using only N_{H_2} , including the regression coefficients and the standardized z -value and p -value for the test of the hypothesis that $\beta_i = 0$.

Predictor	Estimate	Std. error	z -value	p -value
Intercept	-2.66938	0.24205	-11.03	<2e-16
N_{H_2}	0.60880	0.07855	7.75	9.15e-15

where $x_{N_{\text{H}_2}}$ is the beam-averaged H_2 column density in 10^{22} cm^{-3} . The regression summary of this model is shown in Table 4. In general, the results of the binomial model are consistent with the direct investigations outlined above.

4.3. 1.1 mm dust clumps with associated 6.7 GHz class II and/or 95 GHz class I methanol masers.

C2012 suggested that class I methanol masers with and without an associated 6.7 GHz class II methanol maser are different in the dust properties. However, limited by the small sample of 33 sources, they were unable to thoroughly investigate the star formation activities and physical properties of the class I and class II methanol masers.

As stated earlier, the sample of C2012 is covered by our sample, with only a few exceptions without valid data. In total, 194 (sources marked *C* in Table B.1) out of 214 sources in their sample had been studied in both the 6.7 GHz class II and 95 GHz class I methanol maser lines. This allows us to provide more meaningful constraints on the nature of BGPS sources with associated class I and class II methanol masers.

Similarly, the 194 overlapped clumps were split into four subgroups: sources with and without class II methanol masers and sources with and without class I methanol masers. The basic statistical parameters are summarized in Table 5. The trend drawn from the entire sample in the previous section is apparent in this smaller subsample as well. We also found that there is no significant statistical difference between sources with class I methanol masers and those with class II methanol masers, because the two groups share virtually the same mean values of beam-averaged H_2 column density, 1.1 mm integrated flux density, and angular radius.

The 194 clumps with detectable methanol emissions were also split into the following three subgroups: (1) 36 sources in total with both class I and II methanol maser counterparts; (2) 17 sources in total with only class I methanol maser counterparts; and (3) 24 sources in total with only class II methanol maser counterparts. A comparison of the mass, beam-averaged H_2 column density, and integrated flux density for the three subgroups is shown in Fig. 4. The derived statistical parameters are also summarized in Table 5. The first subgroup is found to show the highest mean and median values of mass, column density, and integrated flux (a difference of approximately two standard deviations). Comparing this sample with the smaller sample of C2012, we find that their results remain valid. We additionally find that the distributions of mass, column density, and flux density in the first subgroup cover the widest range. In general, there is no significant difference between the statistical results of the latter two categories.

Since class II methanol masers are thought to exclusively show traces of ongoing high-mass star formations (Walsh et al. 2001; Minier et al. 2003) and since class I methanol masers show traces of both high- and low-mass star formations (Kalenskii et al. 2006, 2010), it is reasonable to expect that sources with detectable class II methanol maser emissions have higher values

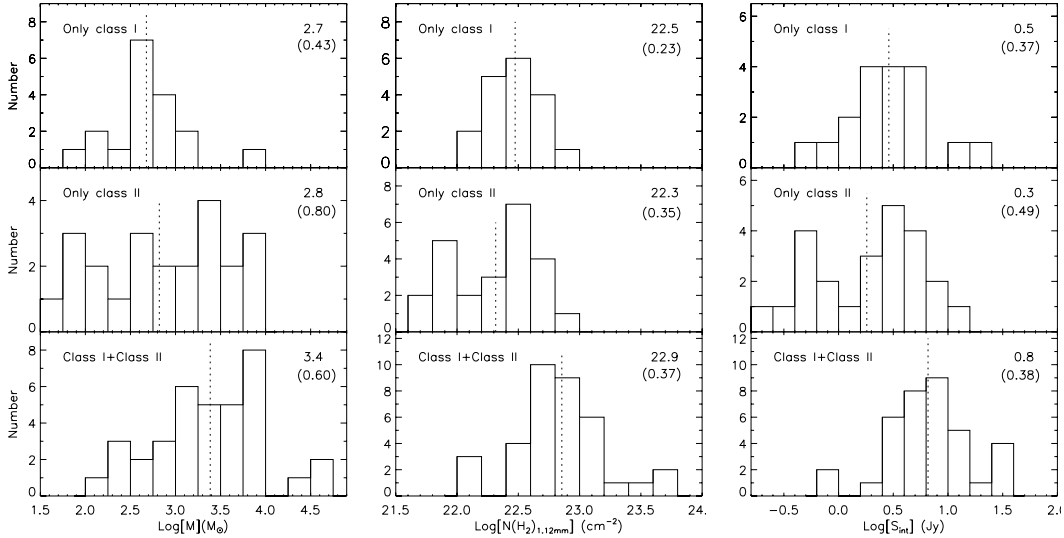


Fig. 4. Distributions of mass (*left*), beam-averaged H_2 column density (*middle*), and 1.1 mm integrated flux density of the BGPS sources (*right*) for the three subgroups with only class I or class II detections and with both class I and class II detections. Together with the standard deviation, the mean value is marked and indicated by a dotted line in each plot.

Table 5. Statistical parameters for sources with and without associated methanol masers for the subsample overlapped with C2012.

Property	Group	Mean	Standard deviation	Minimum	Median	Maximum
$\log[N_{H_2}^{\text{beam}}]$ (cm^{-2})	class I	22.7	0.37	22.0	22.7	23.8
	class II	22.6	0.45	21.7	22.7	23.8
	no class I	22.1	0.27	21.6	22.1	23.0
	no class II	22.1	0.27	21.6	22.1	22.9
$\log[S_{\text{int}}]$ (Jy)	class I	0.7	0.41	-0.2	0.7	1.5
	class II	0.6	0.50	-0.7	0.7	1.5
	no class I	0.1	0.42	-0.8	0.1	1.1
	no class II	0.1	0.42	-0.8	0.1	1.3
Radius ($''$)	class I	60.0	25.10	15.7	58.4	128.7
	class II	58.2	21.82	21.2	58.1	118.2
	no class I	49.2	21.91	5.1	46.1	113.3
	no class II	49.7	23.88	5.1	46.1	128.7
$\log[\text{Mass}]$ (M_{\odot})	only class I	2.7	0.43	1.9	2.7	3.9
	only class II	2.8	0.80	1.2	3.0	4.0
	class I+II	3.4	0.60	2.2	3.4	4.7
$\log[N_{H_2}^{\text{beam}}]$ (cm^{-2})	only class I	22.5	0.23	22.0	22.4	22.9
	only class II	22.3	0.35	21.7	22.4	23.0
	class I+II	22.9	0.37	22.2	22.8	23.8
$\log[S_{\text{int}}]$ (Jy)	only class I	0.5	0.37	-0.2	0.5	1.3
	only class II	0.3	0.49	-0.7	0.4	1.1
	class I+II	0.8	0.38	-0.1	0.8	1.5

of mass, column density and flux density than those with detectable class I methanol maser emissions. However, this alone cannot account for our findings in Fig. 4.

It is important to keep in mind that properties of dust clumps can also change during the course of a maser's evolution. For example, as a maser increases in flux density (and therefore luminosity), the dust clump becomes less dense and it continues to increase in mass, radius, and flux density (proposed by Breen et al. 2010, 2011, and also in this study). Once the evolutionary phase of a maser is taken into account, the situation will become more complicated. Ellingsen (2007) proposed a possible evolutionary sequence for the common maser species (class I and II methanol, water, and OH masers), which has recently been refined and

quantified by Breen et al. (2010). They both proposed that the appearance and disappearance of class I methanol masers precede the class II methanol masers and do not overlap in time with OH masers (Ellingsen 2007; Breen et al. 2010). However, Voronkov et al. (2010) found that class I methanol masers do overlap in time with OH masers, which were thought to have a somewhat more evolved stage. To explain why sources with associated class I methanol masers have fainter red colors than those with associated class II methanol masers, Chen et al. (2011) suggested two epochs of class I methanol maser emission associated with high-mass star formation: an early epoch that significantly overlaps with the class II methanol maser phase, while the latter occurs after the class II methanol maser had

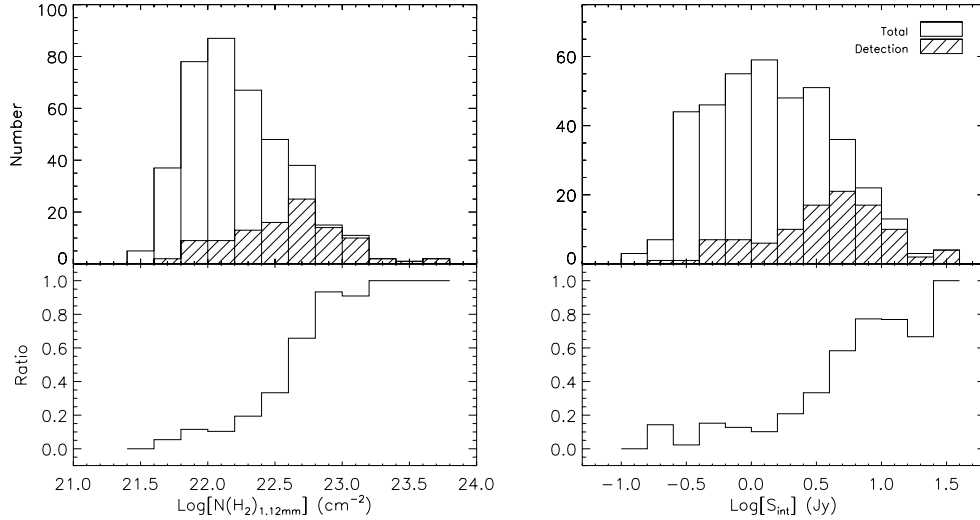


Fig. 5. Detection rates of class II methanol masers versus the BGPS beam-averaged H_2 column density (*left*), and integrated flux density of the BGPS sources (*right*). For each BGPS property, the *upper panel* shows the histogram distributions of total sample sources (blank) and detected 6.7 GHz class II methanol maser sources (hatched), and the *lower panel* shows the corresponding detection rate of class II methanol maser in each statistical bin.

faded out. Both studies suggested that the evolutionary phase of class I methanol masers needs to be revised.

4.4. Detection rates

Our single-dish survey, together with data from the literature, yields a detection rate of 26% of class II methanol masers of a sample of 391 sources with both 1.1 mm dust clump and GLIMPSE point source associations. For our 194 sources overlapped with C2012, the detection rates of class I and class II methanol masers are comparable, which are 28% and 31%, respectively. Generally, our detection rate is slightly lower than that of the other surveys with higher sensitivity, for example, a detection rate of $\sim 35\%$ for a sample of water masers with a sensitivity of 0.1–0.2 Jy (Xu et al. 2008).

To directly compare the relationships between the properties of the associated dust clumps and the detection rates of class II methanol masers, we plot the detection rates of class II methanol masers as a function of the BGPS beam-averaged H_2 column density (*left*) and integrated flux density of the BGPS source (*right*) in Fig. 5. The detection rate is distinctly low in both low column density and low flux density ranges, while it increases dramatically with increasing column density and flux density.

The left panel of Fig. 6 shows the logarithm of the integrated flux density versus the beam-averaged H_2 column density of BGPS sources with and without class II methanol maser associations (marked by red circles and green triangles, respectively) in our sample. The solid lines mark the boundary defined by C2012 in which most (90%) of their class I methanol maser detections are allocated. We find that 81% and 75% of detected class II methanol masers fall into their defined region for the overlapped subsample and the entire sample, respectively. Moreover, sources within their defined region correspond to a class II methanol maser detection rate of 52% for the smaller overlapped subsample, and 45% for the entire sample. To some extent, the new criteria for targeting 95 GHz class I methanol maser searches can also be applied to 6.7 GHz class II methanol maser searches, because the class II methanol maser detection rate is as high as 67% for sources with associated class I methanol maser in this current sample.

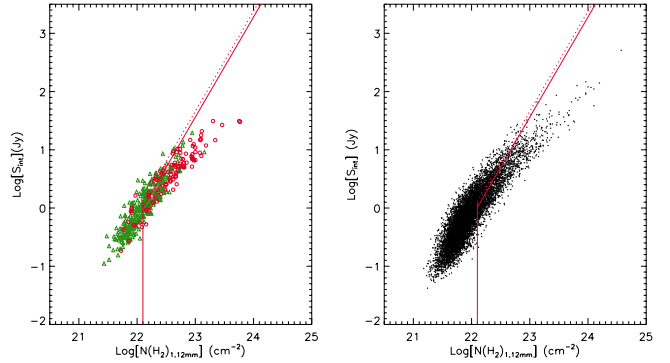


Fig. 6. *Left panel:* logarithm of the integrated flux density versus beam-averaged H_2 column density of BGPS sources with and without class II methanol maser detections (marked by red circles and green triangles, respectively) in our current sample. The solid lines mark the boundary defined by Chen et al. (2012), while the dotted lines mark the slightly revised boundary. *Right panel:* same as *left panel*, but for all BGPS sources.

If the intercept of their defined region were slightly changed from -38 to -37.9 , marked by the dotted line in Fig. 6, we would detect 83% of all expected class II methanol masers of this study, and the sources that fall into the revised region would correspond to a class II methanol maser detection rate of 43%. A comparison of the detection rates of class II methanol masers in different subsamples is summarized in Table 6. Since our sample is much larger, we propose that the revised boundary is as follows:

$$\log(S_{\text{int}}) \leq -37.9 + 1.72 \log(N_{\text{H}_2}^{\text{beam}}), \text{ and } \log(N_{\text{H}_2}^{\text{beam}}) \geq 22.1, \quad (2)$$

which may be more appropriate for efficient methanol maser searches, at least for class II methanol masers. In the right panel of Fig. 6 all BGPS sources are plotted. Approximately 1700 sources are located within the slightly revised boundary and ~ 700 of them are expected to be associated with a class II methanol maser.

5. Summary

We reported results of a 6.7 GHz class II methanol maser survey using the Effelsberg 100 m radio telescope. A sample

Table 6. Detection rates of class II methanol masers in different subsamples.

	Detections	Total numbers	Detection rate
All with valid data ^a	103	391	26%
Overlapped with C2012	60	194	31%
With associated class I methanol masers	36	54	67%
Within the boundary defined by C2012 ^b	78	172	45%
Within the boundary defined by C2012 ^c	49	95	52%
Within the slightly revised boundary ^b	86	200	43%
Within the slightly revised boundary ^c	52	110	47%

Notes. ^(a) A sample of 404 sources from the BGPS 1.1 mm dust clump survey that met specific GLIMPSE point source color criteria was selected, 13 sources of which lacked valid data due to observing time constraints. This reduced our sample size to 391 sources. We observed a total of 318 targets, which resulted in the detection of twenty-nine 6.7 GHz methanol masers at above the 3σ limit. Combining an additional 74 detections directly from the literature (including the variable source detected at about 2σ by us), a total of 103 methanol masers are coincident with the 391 sources. ^(b) The entire sample with valid data. ^(c) The smaller subsample overlapped with C2012.

of 404 BGPS 1.1 mm dust clumps with GLIMPSE point-source associations was selected and 318 were observed. We detected 29 6.7 GHz methanol masers with flux densities in excess of the 3σ detection limit, 12 of which are new discoveries. Combining our results with the 74 detections directly from the literature, a total of 103 methanol masers are coincident with 1.1 mm dust clumps, which means an overall detection rate of 26%, similar to that of Chen et al. (2012).

The analysis of maser and 1.1 mm emissions revealed that the luminosity or flux of 6.7 GHz methanol masers increases with increasing mass or column density of the associated dust clump, whereas it decreases with increasing H_2 number density of the associated dust clump. Our results support the evolutionary scenario presented in Breen et al. (2010).

We carried out a statistical analysis of the properties of the mid-IR and 1.1 mm dust clumps with or without 6.7 GHz class II methanol masers. We found that class II methanol masers are most likely associated with the brighter BGPS source. However, no significant difference between the two groups was found in properties of the mid-IR.

A comparison for the overlapped sample with C2012 of the 1.1 mm dust clump properties revealed that those associated with both class I and II methanol masers have the highest mean and median values of mass, column density, and integrated flux. There is no significant difference between statistical results of those with only class I methanol masers or those with only class II methanol masers. Because our sample is much larger, we revised the boundary defined by C2012 for efficiently selecting BGPS sources with an associated class II methanol maser, in which $\sim 80\%$ of the expected 6.7 GHz class II methanol masers will be detected with a detection rate in the range of 40–50%.

Acknowledgements. We are grateful to the staff of the Effelsberg 100 m radio telescope for their assistance in the observation. We would like to thank Alex Kraus for his help during the process of data calibration. We also thank the anonymous referee for a very helpful report and comments that helped to improve the paper. This work was supported by the National Natural Science Foundation of China (grants Nos. 11003046, 11133008, 11073054, 11233007, 10921063, 11073041 and 11273043), the Strategic Priority Research Program of the Chinese Academy of Sciences (grants Nos. XDA04060701 and XDB09000000), and the Key Laboratory for Radio Astronomy, CAS.

References

Aguirre, J. E., Ginsburg, A. G., Dunham, M. K., et al. 2011, *ApJS*, 192, 4
 Becker, R. H., White, R. L., Helfand, D. J., & Zoonematkermani, S. 1994, *ApJS*, 91, 347
 Breen, S. L., & Ellingsen, S. P. 2011, *MNRAS*, 416, 178
 Breen, S. L., Ellingsen, S. P., Johnston-Hollitt, M., et al. 2007, *MNRAS*, 377, 491

Breen, S. L., Ellingsen, S. P., Caswell, J. L., & Lewis, B. E. 2010, *MNRAS*, 401, 2219
 Breen, S. L., Ellingsen, S. P., Caswell, J. L., et al. 2011, *ApJ*, 733, 80
 Burnham K. P., & Anderson D. R. 2002, *Model Selection and Multimodel Inference, A Practical Information – Theoretic Approach*, 2nd edn. (New York: Springer)
 Caswell, J. L. 2009, *PASA*, 26, 454
 Caswell, J. L., Vaile, R. A., Ellingsen, S. P., Whiteoak, J. B., & Norris, R. P. 1995, *MNRAS*, 272, 96
 Caswell, J. L., Fuller, G. A., Green, J. A., et al. 2010, *MNRAS*, 404, 1029
 Caswell, J. L., Fuller, G. A., Green, J. A., et al. 2011, *MNRAS*, 417, 1964
 Chen, X., Ellingsen, S. P., Shen, Z. Q., Titmarsh, A., & Gan, C. G. 2011, *ApJS*, 196, 9
 Chen, X., Ellingsen, S. P., He, J.-H., et al. 2012, *ApJS*, 200, 5 (C2012)
 Chen, X., Gan, C. G., Ellingsen, S. P., et al. 2013, *ApJS*, 206, 22
 Cyganowski, C. J., Whitney, B. A., Holden, E., et al. 2008, *AJ*, 136, 2391
 Cyganowski, C. J., Brogan, C. L., Hunter, T. R., & Churchwell, E. 2009, *ApJ*, 702, 1615
 Dunham, M. K., Rosolowsky, E., Evans, N. J., II., Cyganowski, C., & Urquhart, J. S. 2011, *ApJ*, 741, 110
 Ellingsen, S. P. 2006, *ApJ*, 638, 241
 Ellingsen, S. P. 2007, *MNRAS*, 377, 571
 Fontani, F., Cesaroni, R., & Furuya, R. S. 2010, *A&A*, 517, A56
 Green, J. A., & McClure-Griffiths, N. M. 2011, *MNRAS*, 417, 2500
 Green, J. A., Caswell, J. L., Fuller, G. A., et al. 2009, *MNRAS*, 392, 783
 Green, J. A., Caswell, J. L., Fuller, G. A., et al. 2010, *MNRAS*, 409, 913
 Green, J. A., Caswell, J. L., Fuller, G. A., et al. 2012, *MNRAS*, 420, 3108
 Heyer, M., Krawczyk, C., Duval, J., & Jackson, J. M. 2009, *ApJ*, 699, 1092
 Kalenskii, S. V., Promyslov, V. G., Slysh, V. I., Bergman, P., & Winnberg, A. 2006, *Astron. Rep.*, 50, 289
 Kalenskii, S. V., Johansson, L. E. B., Bergman, P., et al. 2010, *MNRAS*, 405, 613
 Lee, H. T., Takami, M., Duan, H. Y., et al. 2012, *ApJS*, 200, 2
 Menten, K. M. 1991, *ApJ*, 380, 75
 Minier, V., Ellingsen, S. P., Norris, R. P., & Booth, R. S. 2003, *A&A*, 403, 1095
 Moscadelli, L., Xu, Y., & Chen, X. 2010, *ApJ*, 716, 1356
 Ott, M., Witzel, A., Quirrenbach, A., et al. 1984, *A&A*, 284, 331
 Pandian, J. D., Goldsmith, P. F., & Deshpande, A. A. 2007, *ApJ*, 656, 255
 Pandian, J. D., Momjian, E., Xu, Y., Menten, K. M., & Goldsmith, P. F. 2011, *ApJ*, 730, 55
 Pestalozzi, M. R., Minier, V., & Booth, R. S. 2005, *A&A*, 432, 737
 Reid, M. J., Menten, K. M., Zheng, X. W., et al. 2009, *ApJ*, 700, 137
 Rosolowsky, E., Dunham, M. K., Ginsburg, A., et al. 2010, *ApJS*, 188, 123
 Schlingman, W. M., Shirley, Y. L., Schenk, D. E., et al. 2011, *ApJS*, 195, 14
 Sridharan, T. K., Beuther, H., Schilke, P., Menten, K. M., & Wyrowski, F. 2002, *ApJ*, 566, 931
 Szymczak, M., Hrynek, G., & Kus, A. J. 2000, *A&AS*, 143, 269
 Szymczak, M., Wolak, P., Bartkiewicz, A., & Borkowski, K. M. 2012, *Astron. Nachr.*, 333, 634
 Urquhart, J. S., Hoare, M. G., Purcell, C. R., et al. 2009, *A&A*, 501, 539
 Voronkov, M. A., Caswell, J. L., Ellingsen, S. P., & Sobolev, A. M. 2010, *MNRAS*, 405, 2471
 Walsh, A. J., Bertoldi, F., Burton, M. G., & Nikola, T. 2001, *MNRAS*, 326, 36
 Wood, D. O. S., & Churchwell, E. 1989, *ApJS*, 69, 831
 Wu, Y. W., Xu, Y., Pandian, J. D., et al. 2010, *ApJ*, 720, 392
 Xu, Y., Li, J. J., Hachisuka, K., et al. 2008, *A&A*, 485, 729
 Xu, Y., Voronkov, M. A., Pandian, J. D., et al. 2009, *A&A*, 507, 1117

Appendix A:

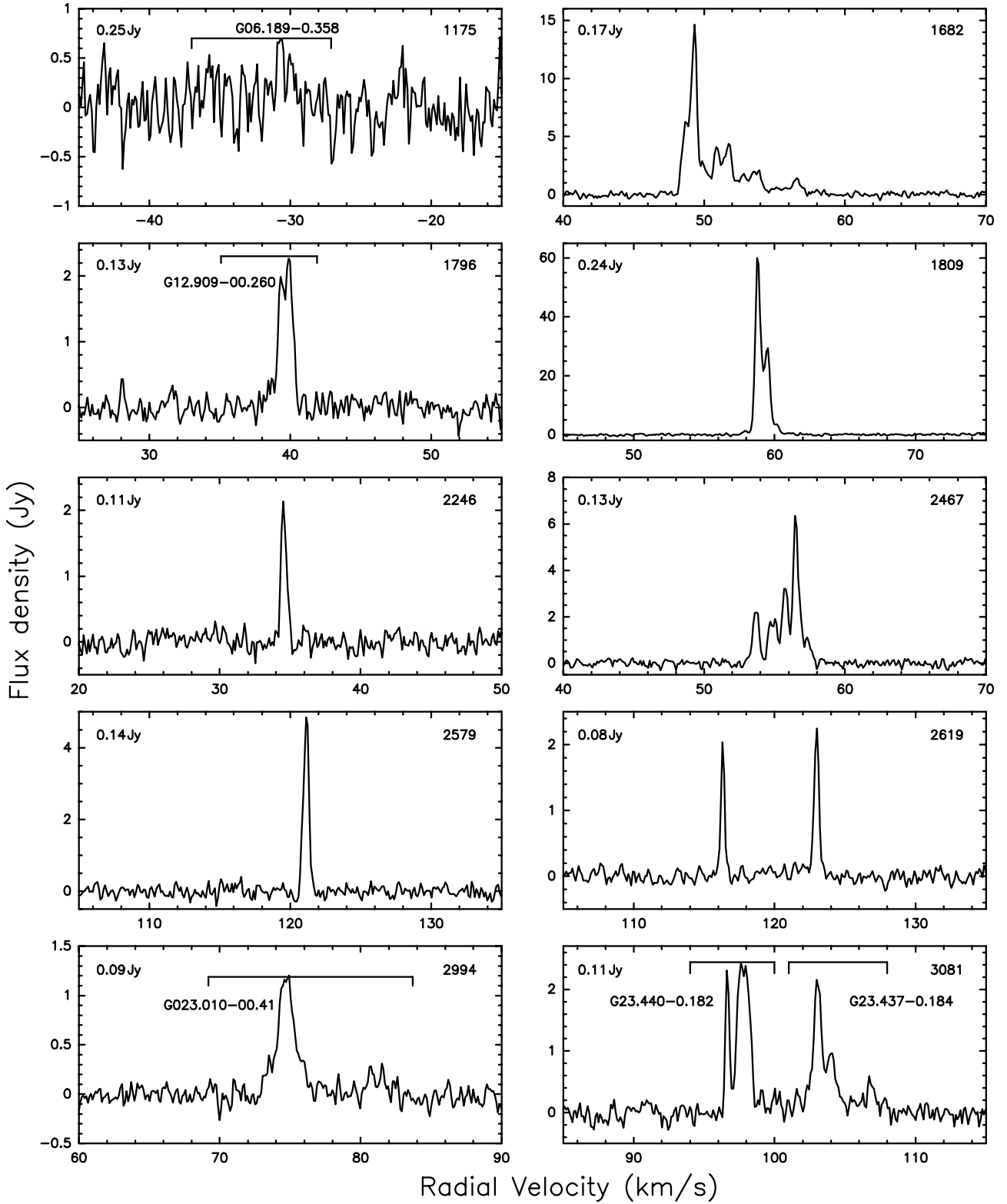


Fig. A.1. Spectra of the 6.7 GHz methanol masers, in units of Jy. The spectral extent is marked in the highly variable source G06.189-0.358 and in seven sources that may have suffered from confusion due to strong adjacent sources. The rms for each spectrum and the PID number of each associated BGPS source are marked in the upper left and upper right corners, respectively. The spectra have a resolution of 0.11 km s^{-1} .

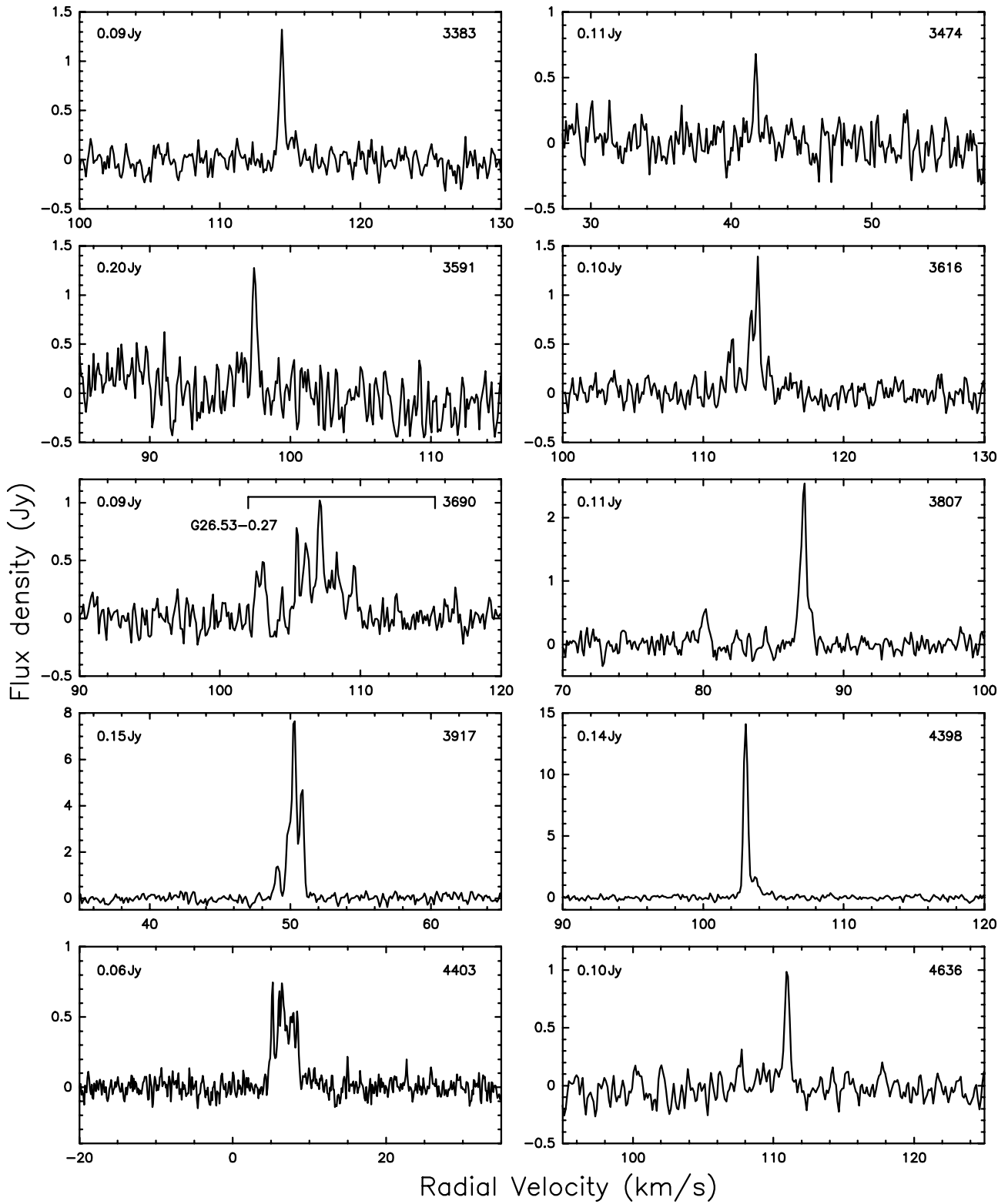


Fig. A.1. continued.

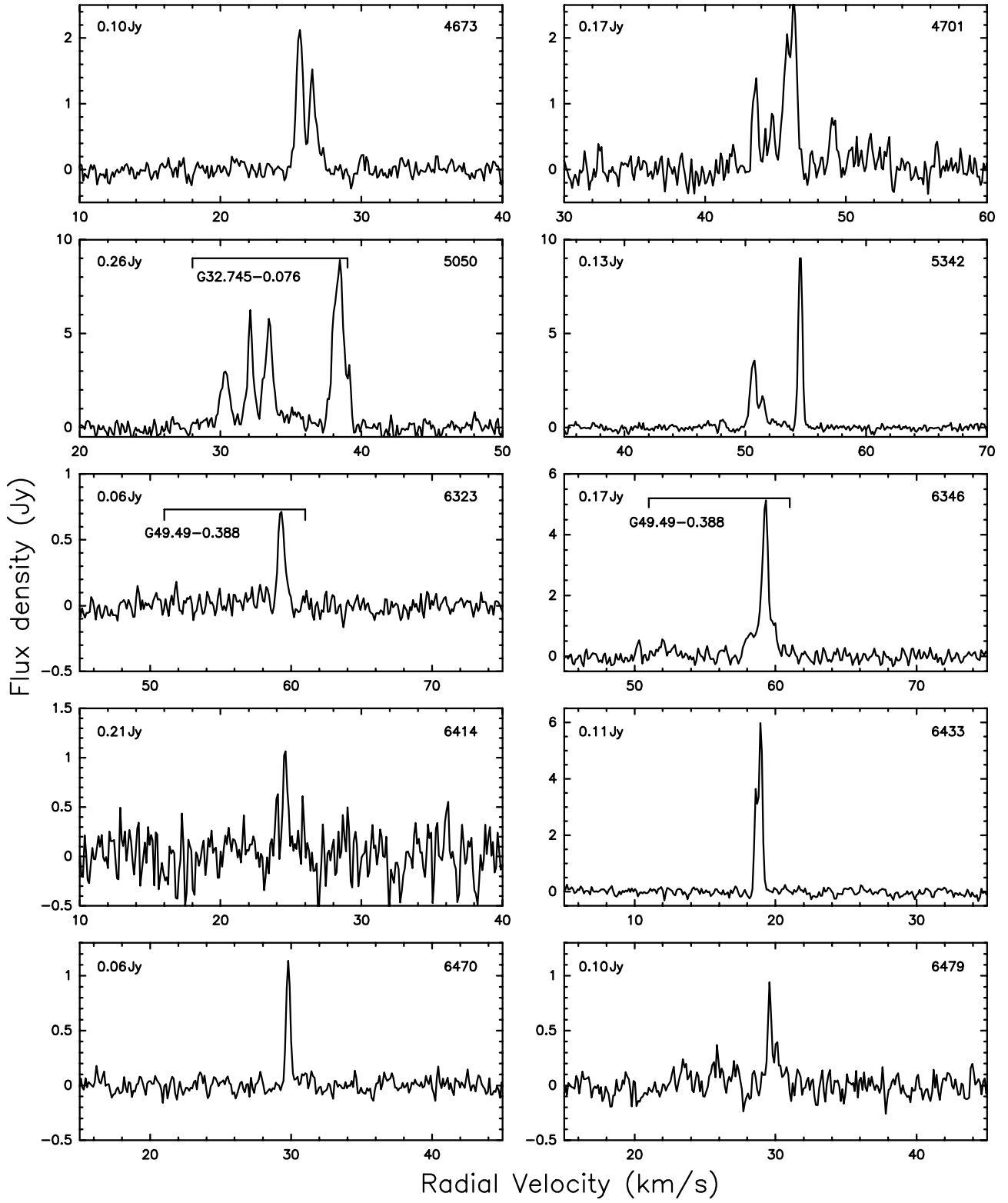


Fig. A.1. continued.

Appendix B:

Table B.1. Parameters of the target BGPS and GLIMPSE sources.

BGPS source								GLIMPSE point source			
PID	Name	RA	Dec	R	$S_{40''}$	S_{int}	N_{H_2}	3.6 μm	4.5 μm	5.8 μm	8.0 μm
(1)	(2)	(J2000)	(J2000)	($''$)	(Jy)	(Jy)	10^{22} cm^{-2}	(mag)	(mag)	(mag)	(mag)
		(3)	(4)	(5)	(6)	(7)	(8)	(9)	(10)	(11)	(12)
1031*	G004.569-00.079	17 56 25.30	-25 03 03.8	59.35	0.134(0.041)	0.645(0.119)	0.81	11.79(0.33)	9.89(0.11)	8.64(0.05)	7.87(0.04)
1047	G004.763+00.089	17 56 12.69	-24 47 56.0	35.09	0.182(0.045)	0.661(0.114)	1.10	12.40(0.11)	10.64(0.07)	9.95(0.07)	9.09(0.07)
1051 ^C	G004.783+00.043	17 56 25.86	-24 48 17.0	27.96	0.175(0.041)	0.422(0.081)	1.06	12.12(0.04)	10.09(0.04)	8.95(0.03)	8.19(0.04)
1053 ^C	G004.803+00.191	17 55 54.71	-24 42 46.7	25.94	0.094(0.038)	0.211(0.065)	0.57	13.30(0.06)	11.06(0.05)	9.99(0.04)	9.56(0.05)
1056	G004.845-00.123	17 57 12.05	-24 50 04.0	21.30	0.103(0.040)	0.310(0.084)	0.62	12.77(0.06)	11.15(0.06)	10.28(0.05)	9.71(0.07)
1059	G004.879-00.155	17 57 23.88	-24 49 15.8	31.28	0.138(0.040)	0.397(0.087)	0.83	13.07(0.09)	11.69(0.06)	10.52(0.07)	10.06(0.11)
1066 ^C	G004.967+00.047	17 56 49.37	-24 38 37.0	–	0.096(0.041)	0.166(0.060)	0.58	13.00(0.05)	10.83(0.06)	9.07(0.03)	7.91(0.02)
1071 ^C	G005.043-00.099	17 57 32.79	-24 39 03.9	57.77	0.157(0.041)	0.553(0.110)	0.95	13.31(0.07)	11.09(0.08)	9.57(0.04)	8.47(0.03)
1073	G005.063-00.275	17 58 15.68	-24 43 18.6	–	0.065(0.035)	0.126(0.049)	0.39	12.65(0.12)	11.18(0.08)	8.89(0.05)	6.93(0.04)
1074	G005.079-00.093	17 57 36.18	-24 37 00.9	47.99	0.215(0.043)	0.845(0.119)	1.30	11.98(0.07)	10.60(0.10)	8.57(0.05)	7.16(0.06)
1084 ^C	G005.333-00.093	17 58 09.70	-24 23 49.2	–	0.087(0.039)	0.198(0.063)	0.53	14.04(0.11)	11.42(0.08)	9.81(0.04)	8.74(0.03)
1087 ^C	G005.361+00.017	17 57 48.30	-24 19 03.8	46.14	0.281(0.041)	0.925(0.119)	1.70	12.39(0.08)	10.21(0.05)	8.76(0.03)	7.82(0.03)
1090 ^C	G005.373+00.319	17 56 41.11	-24 09 21.4	–	0.145(0.036)	0.230(0.054)	0.88	9.55(0.09)	7.45(0.06)	6.00(0.02)	5.37(0.03)
1131 ^C	G005.841-00.379	18 00 21.60	-24 05 56.6	–	0.107(0.058)	0.203(0.091)	0.65	13.34(0.09)	10.99(0.06)	9.17(0.04)	8.01(0.04)
1142	G005.911-00.543	18 01 08.17	-24 07 10.6	18.23	0.419(0.074)	0.918(0.145)	2.53	11.62(0.08)	9.72(0.06)	8.56(0.04)	7.97(0.03)
1144*	G005.931-00.425	18 00 43.83	-24 02 37.5	–	0.201(0.074)	0.314(0.102)	1.21	13.29(0.08)	11.60(0.10)	10.46(0.07)	9.61(0.09)
1164 ^C	G006.057-00.029	17 59 30.07	-23 44 15.4	–	0.116(0.043)	0.233(0.069)	0.70	13.55(0.15)	10.50(0.09)	8.69(0.04)	7.70(0.04)
1175*	G006.191-00.359	18 01 02.63	-23 47 06.9	48.27	1.455(0.104)	4.638(0.339)	8.78	10.93(0.08)	8.50(0.14)	7.54(0.03)	7.26(0.03)
1203 ^C	G006.407-00.039	18 00 17.92	-23 26 20.2	5.13	0.126(0.039)	0.246(0.062)	0.76	14.21(0.17)	10.98(0.07)	9.43(0.04)	8.71(0.03)
1234	G006.745-00.221	18 01 43.03	-23 14 08.1	23.96	0.108(0.036)	0.257(0.068)	0.65	14.24(0.26)	12.77(0.11)	9.78(0.10)	8.47(0.15)
1240*	G006.799-00.255	18 01 57.72	-23 12 19.6	40.78	1.663(0.115)	4.416(0.321)	10.04	10.00(0.08)	8.03(0.06)	6.65(0.02)	5.70(0.03)
1250	G006.919-00.225	18 02 06.39	-23 05 10.7	67.93	0.826(0.072)	4.245(0.328)	4.99	11.86(0.05)	9.98(0.05)	9.11(0.04)	8.61(0.04)
1251 ^C	G006.923-00.251	18 02 12.80	-23 05 44.4	36.42	0.441(0.059)	1.453(0.164)	2.66	10.33(0.06)	8.24(0.06)	6.74(0.03)	5.72(0.02)
1259 ^C	G007.013-00.253	18 02 24.84	-23 01 06.2	36.39	0.327(0.042)	0.956(0.114)	1.97	12.49(0.13)	10.01(0.08)	8.71(0.09)	7.68(0.28)
1289 ^C	G007.335-00.567	18 04 17.39	-22 53 33.5	37.71	0.455(0.059)	1.366(0.159)	2.75	12.13(0.09)	9.94(0.06)	8.67(0.04)	7.87(0.02)
1341 ^C	G008.206+00.192	18 03 16.99	-21 45 39.3	41.18	0.222(0.063)	0.691(0.155)	1.34	15.42(0.34)	11.89(0.06)	10.12(0.04)	9.30(0.04)
1346 ^C	G008.274+00.512	18 02 13.75	-21 32 38.4	–	0.159(0.066)	0.243(0.088)	0.96	12.95(0.14)	11.21(0.14)	9.99(0.06)	9.12(0.06)
1352 ^{C*}	G008.326-00.096	18 04 37.05	-21 47 52.5	–	0.237(0.060)	0.349(0.092)	1.43	11.40(0.04)	9.89(0.04)	8.85(0.03)	8.22(0.04)
1360 ^C	G008.422-00.274	18 05 29.32	-21 48 05.0	65.48	0.616(0.073)	3.268(0.309)	3.72	13.68(0.08)	11.52(0.08)	10.20(0.07)	9.72(0.20)
1361 ^C	G008.440-00.168	18 05 07.71	-21 44 01.7	–	0.140(0.064)	0.211(0.085)	0.84	10.58(0.05)	8.93(0.06)	7.64(0.04)	6.96(0.03)
1362 ^C	G008.454-00.290	18 05 36.97	-21 46 52.7	16.12	0.217(0.065)	0.478(0.120)	1.31	14.17(0.08)	11.72(0.06)	10.19(0.04)	9.57(0.05)
1363 ^C	G008.458-00.224	18 05 22.60	-21 44 43.9	32.57	0.367(0.062)	1.016(0.150)	2.22	12.68(0.07)	11.25(0.07)	9.98(0.05)	9.37(0.04)
1380 ^C	G008.710-00.414	18 06 37.21	-21 37 06.6	43.96	0.558(0.072)	2.237(0.214)	3.37	14.85(0.11)	11.97(0.06)	10.65(0.06)	9.94(0.05)
1395 ^{C*}	G008.832-00.028	18 05 25.71	-21 19 24.6	70.29	0.913(0.081)	3.865(0.340)	5.51	11.93(0.35)	9.73(0.20)	9.10(0.07)	9.02(0.05)
1405 ^C	G008.956+00.186	18 04 53.31	-21 06 38.1	43.89	0.186(0.057)	0.685(0.142)	1.12	13.32(0.07)	10.75(0.08)	9.42(0.03)	8.33(0.02)
1407 ^C	G009.028-00.310	18 06 53.76	-21 17 24.6	14.70	0.137(0.062)	0.329(0.108)	0.83	14.00(0.09)	11.88(0.09)	10.73(0.05)	10.16(0.08)
1409 ^C	G009.125-00.002	18 05 56.88	-21 03 15.6	14.91	0.117(0.059)	0.275(0.096)	0.71	11.95(0.11)	10.28(0.07)	9.19(0.03)	8.60(0.02)
1412 ^{C*}	G009.212-00.202	18 06 52.57	-21 04 36.8	64.29	1.018(0.088)	4.599(0.368)	6.14	12.04(0.05)	9.62(0.06)	8.64(0.04)	8.80(0.09)
1421*	G009.620+00.194	18 06 14.92	-20 31 39.2	46.92	3.638(0.232)	9.744(0.645)	21.96	13.23(0.09)	11.77(0.21)	9.40(0.08)	7.74(0.11)
1425 ^C	G009.850-00.032	18 07 34.20	-20 26 12.9	35.30	0.210(0.063)	0.787(0.154)	1.27	10.89(0.05)	8.77(0.05)	7.66(0.03)	6.63(0.02)
1428	G009.880-00.110	18 07 55.39	-20 26 55.1	40.25	0.204(0.059)	0.715(0.144)	1.23	13.56(0.07)	12.00(0.07)	10.99(0.07)	9.60(0.05)
1442	G010.050-00.208	18 08 38.47	-20 20 51.5	36.32	0.173(0.051)	0.619(0.120)	1.04	13.03(0.07)	11.63(0.09)	10.53(0.05)	9.92(0.03)
1458	G010.190+00.096	18 07 47.90	-20 04 39.4	–	0.111(0.050)	0.250(0.083)	0.67	13.20(0.17)	11.83(0.16)	10.04(0.11)	8.81(0.14)
1466 ^{C*}	G010.214-00.324	18 09 24.77	-20 15 37.6	84.60	1.556(0.134)	8.300(0.634)	9.39	12.93(0.08)	10.25(0.08)	8.44(0.04)	6.81(0.04)
1467 ^C	G010.226-00.208	18 09 00.30	-20 11 37.5	98.76	0.997(0.083)	7.897(0.576)	6.02	12.47(0.07)	10.23(0.05)	8.80(0.04)	7.68(0.04)
1472 ^C	G010.262+00.074	18 08 01.76	-20 01 31.4	64.92	0.240(0.067)	1.312(0.227)	1.45	13.60(0.14)	11.57(0.15)	9.96(0.22)	8.59(0.19)
1479 ^{C*}	G010.320-00.258	18 09 23.13	-20 08 08.7	62.32	0.857(0.074)	3.361(0.277)	5.17	11.41(0.12)	8.85(0.11)	7.23(0.09)	6.00(0.30)
1497 ^{C*}	G010.472+00.026	18 08 38.51	-19 51 54.5	37.59	9.398(0.580)	20.789(1.314)	56.72	12.48(0.12)	9.98(0.09)	7.83(0.08)	6.05(0.08)
1506	G010.619-00.440	18 10 40.79	-19 57 40.1	16.57	0.403(0.075)	0.988(0.158)	2.43	9.71(0.04)	7.93(0.04)	6.64(0.03)	5.99(0.03)
1508 ^{C*}	G010.625-00.384	18 10 29.00	-19 55 44.0	31.39	9.722(0.597)	20.020(1.256)	58.68	11.40(0.10)	9.32(0.24)	7.78(0.12)	6.28(0.12)
1516 ^C	G010.670-00.198	18 09 53.11	-19 47 55.7	49.89	0.275(0.047)	1.295(0.152)	1.66	14.73(0.20)	12.29(0.10)	10.81(0.17)	10.10(0.28)
1526	G010.723-00.150	18 09 48.80	-19 43 48.3	–	0.120(0.048)	0.435(0.103)	0.72	14.48(0.21)	12.65(0.20)	10.35(0.11)	8.63(0.11)
1531	G010.743-00.296	18 10 23.86	-19 46 59.1	43.49	0.102(0.044)	0.502(0.111)	0.62	10.83(0.06)	9.07(0.04)	7.82(0.06)	7.17(0.04)
1543 ^{C*}	G010.825-00.102	18 09 50.65	-19 37 03.3	–	0.119(0.043)	0.182(0.056)	0.72	9.67(0.06)	7.59(0.05)	6.45(0.03)	5.81(0.03)
1558	G010.947-00.348	18 11 00.55	-19 37 46.1	44.10	0.105(0.039)	0.408(0.098)	0.63	12.52(0.07)	10.65(0.12)	9.81(0.05)	9.57(0.06)
1559 ^{C*}	G010.959+00.020	18 09 39.95	-19 26 28.8	49.81	0.783(0.073)	2.702(0.239)	4.73	11.15(0.10)	8.73(0.15)	7.05(0.08)	5.53(0.08)
1568	G010.997-00.174	18 10 27.87	-19 30 06.4	58.57	0.169(0.041)	0.907(0.131)	1.02	13.27(0.09)	11.75(0.08)	10.49(0.08)	9.76(0.11)

Notes. Column (1): the ID number of BGPS source, sources overlapped with C2012 and previous methanol maser detections are marked *C* and *, sources without valid data due to the amount of available observation time are marked †. Column (2): name of BGPS source. Columns (3) and (4): positions of 1.1 mm emission peak. Column (5): radius of BGPS source, sources unresolved by BGPS are indicated with –. Columns (6) and (7): the aperture flux density within 40'' and integrated flux density of the BGPS source. Note that a flux calibration correction factor of 1.5 needs to be applied to both the aperture and integrated flux densities listed here to calculate gas mass and column/volume density. Column (8): beam-averaged H₂ column density. Columns (9)–(12): magnitude of the GLIMPSE point source in the 3.6, 4.5, 5.8, and 8.0 μm bands, respectively.

Table B.1. continued.

BGPS source								GLIMPSE point source			
PID	Name	RA (J2000)	Dec (J2000)	R (")	$S_{40''}$ (Jy)	S_{int} (Jy)	N_{H_2} 10^{22} cm^{-2}	3.6 μm (mag)	4.5 μm (mag)	5.8 μm (mag)	8.0 μm (mag)
(1)	(2)	(3)	(4)	(5)	(6)	(7)	(8)	(9)	(10)	(11)	(12)
1580 ^C	G011.063-00.096	18 10 18.59	-19 24 22.7	77.96	0.343(0.047)	2.633(0.234)	2.07	13.66(0.10)	11.20(0.07)	9.98(0.05)	9.52(0.05)
1587 ^C	G011.101+00.072	18 09 45.84	-19 17 30.8	-	0.130(0.043)	0.327(0.077)	0.78	13.95(0.14)	11.60(0.13)	10.21(0.09)	9.12(0.07)
1591 ^C	G011.115+00.052	18 09 52.01	-19 17 21.5	-	0.282(0.046)	0.548(0.085)	1.70	9.71(0.06)	6.83(0.06)	5.26(0.05)	4.35(0.03)
1592 ^{C*}	G011.121-00.128	18 10 32.84	-19 22 15.5	68.78	0.440(0.048)	2.674(0.222)	2.66	14.02(0.14)	11.59(0.09)	10.48(0.06)	9.80(0.05)
1593	G011.147+00.054	18 09 55.50	-19 15 37.1	28.62	0.078(0.041)	0.205(0.070)	0.47	12.31(0.06)	10.57(0.07)	8.90(0.07)	7.80(0.07)
1604	G011.245-00.318	18 11 30.39	-19 21 14.0	-	0.088(0.041)	0.212(0.071)	0.53	13.61(0.10)	11.65(0.07)	10.42(0.07)	9.83(0.06)
1618	G011.467-00.142	18 11 18.34	-19 04 28.5	49.68	0.138(0.039)	0.620(0.109)	0.83	11.68(0.09)	10.13(0.09)	8.60(0.05)	7.55(0.06)
1627	G011.599-00.132	18 11 32.25	-18 57 14.7	27.16	0.197(0.040)	0.509(0.087)	1.19	12.77(0.09)	10.89(0.08)	9.80(0.06)	9.39(0.06)
1630	G011.635-00.064	18 11 21.53	-18 53 23.3	18.83	0.109(0.040)	0.224(0.067)	0.66	10.78(0.31)	9.47(0.17)	8.15(0.09)	6.45(0.07)
1653	G011.895-00.220	18 12 27.90	-18 44 12.8	39.89	0.258(0.051)	0.869(0.128)	1.56	13.41(0.11)	11.50(0.11)	10.27(0.06)	9.42(0.08)
1657 ^{C*}	G011.941-00.154	18 12 18.83	-18 39 53.4	39.10	0.530(0.062)	1.696(0.178)	3.20	12.26(0.09)	10.09(0.08)	8.96(0.04)	8.74(0.06)
1668 ^C	G012.023-00.206	18 12 40.36	-18 37 04.4	37.95	0.352(0.054)	0.969(0.138)	2.12	12.96(0.10)	10.79(0.20)	9.25(0.05)	8.80(0.05)
1679	G012.155-00.136	18 12 40.85	-18 28 06.6	32.96	0.115(0.039)	0.350(0.082)	0.69	9.39(0.10)	7.59(0.06)	6.29(0.05)	5.72(0.09)
1682 ^{C*}	G012.201-00.034	18 12 23.81	-18 22 45.0	52.77	0.694(0.076)	2.064(0.237)	4.19	10.50(0.18)	7.67(0.11)	6.30(0.04)	5.95(0.10)
1699 ^C	G012.367+00.510	18 10 43.55	-17 58 18.5	-	0.078(0.049)	0.103(0.052)	0.47	13.32(0.07)	11.54(0.07)	10.59(0.08)	9.67(0.08)
1708	G012.403-00.466	18 14 24.19	-18 24 32.1	45.78	0.563(0.060)	1.990(0.192)	3.40	8.57(0.11)	6.92(0.07)	5.62(0.03)	5.03(0.04)
1720 ^C	G012.497-00.222	18 13 41.39	-18 12 34.7	42.00	0.438(0.051)	1.341(0.147)	2.64	11.55(0.07)	9.03(0.06)	7.85(0.05)	7.85(0.05)
1727	G012.555-00.348	18 14 16.36	-18 13 08.4	36.32	0.198(0.044)	0.677(0.107)	1.20	13.91(0.09)	12.27(0.10)	11.21(0.11)	9.94(0.06)
1734 ^C	G012.593-00.382	18 14 28.49	-18 12 06.8	-	0.072(0.039)	0.192(0.064)	0.43	13.55(0.14)	11.55(0.09)	10.48(0.08)	9.95(0.10)
1740	G012.621+00.514	18 11 13.54	-17 44 50.4	32.14	0.120(0.046)	0.326(0.089)	0.72	12.38(0.08)	10.63(0.07)	9.34(0.05)	8.34(0.07)
1742 ^{C*}	G012.627-00.016	18 13 11.47	-17 59 48.6	78.87	1.146(0.085)	5.708(0.413)	6.92	11.42(0.06)	7.87(0.07)	6.54(0.04)	6.26(0.04)
1747 [*]	G012.681-00.182	18 13 54.77	-18 01 44.3	86.15	2.086(0.144)	11.822(0.791)	12.59	11.38(0.09)	9.64(0.30)	8.33(0.05)	6.83(0.08)
1749	G012.686-00.282	18 14 17.66	-18 04 17.5	-	0.115(0.050)	0.255(0.084)	0.69	10.64(0.04)	9.17(0.05)	7.97(0.04)	7.32(0.03)
1752	G012.695+00.350	18 11 58.74	-17 45 41.1	16.57	0.156(0.043)	0.374(0.082)	0.94	12.24(0.07)	10.62(0.09)	9.45(0.06)	8.56(0.11)
1753	G012.699+00.474	18 11 31.84	-17 41 53.7	32.14	0.283(0.048)	0.666(0.102)	1.71	12.30(0.12)	10.43(0.05)	9.07(0.05)	8.33(0.18)
1756 ^C	G012.709+00.064	18 13 03.68	-17 53 11.4	-	0.082(0.046)	0.185(0.070)	0.49	11.26(0.19)	9.21(0.08)	7.74(0.03)	6.95(0.05)
1778 ^C	G012.805-00.318	18 14 39.87	-17 59 06.4	72.81	0.664(0.070)	3.174(0.301)	4.01	12.19(0.13)	9.66(0.15)	7.89(0.05)	6.43(0.08)
1796	G012.861-00.272	18 14 36.43	-17 54 50.2	-	0.690(0.086)	1.373(0.172)	4.16	9.61(0.05)	7.91(0.04)	6.69(0.03)	5.99(0.03)
1803 ^{C*}	G012.889+00.490	18 11 51.33	-17 31 26.4	53.31	2.534(0.173)	7.895(0.564)	15.29	12.08(0.10)	8.44(0.19)	6.57(0.04)	6.15(0.05)
1809 ^{C*}	G012.905-00.030	18 13 48.16	-17 45 34.4	65.04	1.032(0.077)	3.558(0.271)	6.23	15.31(0.32)	12.65(0.16)	10.03(0.05)	8.21(0.05)
1841 ^C	G013.037-00.318	18 15 07.81	-17 46 52.7	50.18	0.177(0.046)	0.652(0.116)	1.07	12.49(0.06)	10.19(0.05)	8.98(0.04)	8.39(0.05)
1853 ^C	G013.097-00.146	18 14 36.96	-17 38 47.2	59.34	0.445(0.056)	1.887(0.199)	2.69	10.16(0.06)	7.53(0.05)	6.10(0.03)	5.30(0.03)
1857 ^C	G013.121-00.094	18 14 28.34	-17 36 01.8	64.68	0.386(0.048)	2.208(0.206)	2.33	11.02(0.06)	8.62(0.05)	7.67(0.04)	7.04(0.04)
1865 ^{C*}	G013.179+00.060	18 14 01.29	-17 28 33.3	58.37	1.423(0.108)	5.123(0.378)	8.59	11.23(0.08)	8.90(0.06)	7.63(0.03)	6.78(0.03)
1876	G013.245-00.084	18 14 41.05	-17 29 12.5	62.10	0.944(0.082)	3.541(0.299)	5.70	12.73(0.07)	11.08(0.08)	8.99(0.03)	6.89(0.02)
1877 ^C	G013.245+00.158	18 13 47.59	-17 22 15.8	13.18	0.123(0.044)	0.276(0.076)	0.74	14.72(0.16)	12.02(0.08)	10.07(0.05)	8.70(0.06)
1888	G013.298-00.402	18 15 57.88	-17 35 27.9	52.60	0.086(0.056)	0.480(0.133)	0.52	12.25(0.07)	10.51(0.06)	9.13(0.05)	7.82(0.04)
1900	G013.359-00.030	18 14 42.82	-17 21 39.2	-	0.095(0.050)	0.143(0.062)	0.57	13.46(0.10)	11.59(0.08)	10.57(0.07)	10.01(0.06)
1935	G013.766+00.177	18 14 45.97	-16 54 16.7	22.50	0.149(0.060)	0.336(0.104)	0.90	12.88(0.17)	11.18(0.09)	9.84(0.06)	9.18(0.04)
1962	G013.901-00.515	18 17 34.79	-17 06 55.2	65.78	0.545(0.077)	2.803(0.295)	3.29	13.09(0.07)	11.21(0.07)	10.30(0.06)	9.18(0.05)
1998 ^C	G014.107-00.563	18 18 09.86	-16 57 23.7	15.68	0.593(0.000)	1.247(0.178)	3.58	14.33(0.11)	11.92(0.06)	10.62(0.09)	9.54(0.10)
2002 ^C	G014.133-00.521	18 18 03.65	-16 54 49.7	39.36	0.241(0.093)	1.071(0.225)	1.45	13.47(0.10)	10.91(0.10)	10.26(0.06)	8.86(0.05)
2012 ^C	G014.195-00.509	18 18 08.35	-16 51 12.7	50.13	0.618(0.088)	2.854(0.268)	3.73	14.60(0.11)	11.97(0.09)	10.85(0.06)	10.01(0.08)
2016 [*]	G014.227-00.513	18 18 13.03	-16 49 38.0	69.42	2.016(0.151)	9.750(0.703)	12.17	13.99(0.08)	12.43(0.10)	8.96(0.08)	7.11(0.10)
2019	G014.244-00.071	18 16 37.61	-16 36 07.4	49.38	0.904(0.085)	2.947(0.273)	5.46	12.42(0.09)	10.52(0.14)	9.69(0.08)	9.14(0.09)
2045 ^C	G014.450-00.101	18 17 08.68	-16 26 05.7	96.53	1.030(0.091)	8.996(0.636)	6.22	11.50(0.14)	9.42(0.09)	7.86(0.05)	6.89(0.05)
2048	G014.456-00.183	18 17 27.46	-16 28 06.5	33.32	0.175(0.071)	0.604(0.147)	1.06	13.00(0.09)	11.42(0.13)	9.43(0.05)	7.78(0.10)
2051	G014.474-00.007	18 16 50.82	-16 22 09.2	83.73	0.535(0.064)	3.874(0.331)	3.23	12.86(0.08)	11.00(0.10)	8.82(0.06)	7.32(0.10)
2063	G014.568-00.026	18 17 06.36	-16 17 45.4	57.85	0.207(0.051)	0.964(0.155)	1.25	14.22(0.19)	12.56(0.15)	10.99(0.24)	10.06(0.10)
2067	G014.587-00.406	18 18 32.24	-16 27 35.7	48.82	0.206(0.044)	0.794(0.125)	1.24	12.50(0.09)	9.70(0.10)	8.11(0.03)	7.66(0.04)
2071	G014.601-00.542	18 19 03.90	-16 30 42.4	46.68	0.415(0.076)	1.656(0.223)	2.50	11.87(0.05)	10.20(0.05)	9.20(0.05)	9.05(0.04)
2081 [*]	G014.633-00.574	18 19 14.74	-16 29 55.2	72.46	2.053(0.156)	10.197(0.740)	12.39	13.10(0.06)	11.13(0.07)	10.09(0.06)	9.44(0.09)
2082	G014.634+00.308	18 16 00.72	-16 04 45.7	48.21	0.681(0.068)	2.342(0.224)	4.11	11.47(0.06)	9.98(0.11)	8.86(0.08)	8.24(0.17)
2091 ^C	G014.678-00.044	18 17 23.36	-16 12 27.4	-	0.115(0.059)	0.171(0.070)	0.69	13.66(0.21)	11.43(0.07)	9.80(0.07)	8.77(0.10)
2094	G014.690+00.032	18 17 08.05	-16 09 39.7	99.01	0.277(0.048)	2.569(0.275)	1.67	11.65(0.07)	10.07(0.10)	8.84(0.05)	8.02(0.04)
2096 ^C	G014.708-00.154	18 17 51.12	-16 13 59.8	61.14	0.402(0.063)	2.021(0.220)	2.43	11.41(0.07)	9.33(0.08)	8.26(0.06)	7.26(0.04)
2111	G014.777-00.334	18 18 38.81	-16 15 30.5	29.02	0.239(0.052)	0.604(0.112)	1.44	11.51(0.13)	9.99(0.11)	7.88(0.04)	5.93(0.05)
2117	G014.820+00.080	18 17 12.88	-16 01 25.8	16.66	0.118(0.048)	0.287(0.086)	0.71	12.93(0.08)	11.06(0.07)	9.99(0.05)	9.20(0.09)
2124 ^C	G014.849-00.992	18 21 12.49	-16 30 17.5	56.03	0.883(0.101)	2.881(0.332)	5.33	13.22(0.15)	10.72(0.12)	10.17(0.08)	9.43(0.05)
2149	G014.990-00.014	18 17 53.65	-15 55 07.0	46.68	0.225(0.056)	0.989(0.155)	1.36	12.43(0.10)	10.97(0.07)	9.80(0.06)	9.14(0.05)
2154 ^C	G015.029+00.852	18 14 48.38	-15 28 20.0	28.59	0.243(0.084)	0.595(0.155)	1.47	13.18(0.09)	10.44(0.06)	9.11(0.04)	8.27(0.03)
2177	G015.127-00.494	18 19 55.30	-16 01 31.3	39.00	0.317(0.058)	0.908(0.142)	1.91	13.04(0.06)	11.52(0.09)	9.98(0.07)	8.37(0.10)
2189	G015.182-00.158	18 18 47.95	-15 49 03.0	64.98	0.514(0.061)	2.282(0.238)	3.10	10.67(0.31)	8.86(0.18)	7.26(0.07)	6.01(0.09)
2199 ^C	G015.258-00.156	18 18 56.46	-15 44 58.5	-	0.112(0.057)	0.235(0.089)	0.68	12.15(0.07)	9.23(0.05)	7.86(0.03)	6.96(0.04)
2208	G015.320-00.044	18 18 39.15	-15 38 31.3	-	0.066(0.052)	0.216(0.091)	0.40	12.30(0.07)	11.01(0.06)	9.51(0.04)	8.28(0.03)
2223	G015.532-00.405	18 20 23.62	-15 37 33.0	41.66	0.338(0.061)	1.219(0.165)	2.04	12.34(0.09)	10.65(0.06)	9.67(0.06)	8.77(0.04)
2246 ^{C*}	G016.114-00.301	18 21 08.91	-15 03 48.2	38.80	0.116(0.048)	0.383(0.103)	0.70	10.50(0.13)	8.06(0.06)	6.53(0.03)	5.67(0.03)
2262	G016.302-00.367	18 21 45.33	-14 55 42.4	88.76	0.225(0.048)	1.792(0.219)	1.36	12.21(0.09)	10.32(0.09)	8.80(0.05)	7.78(0.10)

Table B.1. continued.

BGPS source									GLIMPSE point source			
PID	Name	RA (J2000)	Dec (J2000)	R (")	$S_{40''}$ (Jy)	S_{int} (Jy)	N_{H_2} 10^{22} cm^{-2}	$3.6 \mu\text{m}$ (mag)	$4.5 \mu\text{m}$ (mag)	$5.8 \mu\text{m}$ (mag)	$8.0 \mu\text{m}$ (mag)	
(1)	(2)	(3)	(4)	(5)	(6)	(7)	(8)	(9)	(10)	(11)	(12)	
2264 ^C	G016.317-00.533	18 22 23.37	-14 59 38.3	30.48	0.319(0.073)	0.845(0.157)	1.93	11.89(0.06)	9.57(0.05)	8.36(0.04)	7.56(0.03)	
2269	G016.332-00.457	18 22 08.56	-14 56 39.1	36.41	0.132(0.060)	0.384(0.126)	0.80	10.21(0.07)	8.61(0.05)	7.60(0.04)	7.11(0.03)	
2272	G016.359-00.073	18 20 47.66	-14 44 20.7	32.53	0.266(0.063)	0.738(0.137)	1.61	14.97(0.28)	13.00(0.14)	9.93(0.09)	8.21(0.10)	
2292 ^{C*}	G016.586-00.051	18 21 09.21	-14 31 45.5	31.69	1.451(0.115)	3.424(0.292)	8.76	12.72(0.13)	9.33(0.15)	7.69(0.05)	7.43(0.10)	
2297 ^C	G016.641-00.119	18 21 30.62	-14 30 42.6	25.67	0.271(0.068)	0.809(0.155)	1.64	12.22(0.10)	9.88(0.12)	8.80(0.05)	8.31(0.04)	
2305	G016.738-00.091	18 21 35.67	-14 24 50.2	47.61	0.250(0.071)	1.052(0.192)	1.51	14.00(0.12)	12.28(0.09)	10.90(0.10)	9.86(0.07)	
2307	G016.798+00.124	18 20 55.87	-14 15 37.4	41.11	0.279(0.063)	0.928(0.152)	1.68	10.93(0.06)	9.17(0.05)	8.00(0.03)	7.10(0.03)	
2330 [*]	G017.030-00.070	18 22 05.25	-14 08 48.3	35.82	0.351(0.075)	0.996(0.186)	2.12	12.02(0.09)	10.19(0.06)	8.75(0.04)	7.65(0.10)	
2338	G017.225-00.100	18 22 34.56	-13 59 15.9	30.87	0.152(0.072)	0.522(0.147)	0.92	12.63(0.11)	10.76(0.06)	9.83(0.06)	9.09(0.05)	
2348	G017.596+00.090	18 22 35.96	-13 34 18.8	-	0.256(0.073)	0.529(0.133)	1.55	12.93(0.10)	11.10(0.10)	10.05(0.12)	9.19(0.13)	
2354 ^C	G017.856+00.120	18 20 59.50	-13 19 41.4	-	0.118(0.069)	0.182(0.083)	0.71	10.77(0.07)	8.74(0.05)	7.62(0.03)	6.98(0.03)	
2358	G017.960+00.080	18 23 20.23	-13 15 18.1	26.35	0.478(0.088)	1.210(0.186)	2.89	9.81(0.11)	7.98(0.07)	6.70(0.03)	5.73(0.07)	
2365	G018.091-00.302	18 24 58.72	-13 19 01.2	71.23	0.762(0.083)	5.071(0.410)	4.60	12.67(0.09)	10.98(0.08)	10.02(0.05)	9.41(0.09)	
2369	G018.108+00.370	18 22 34.20	-12 59 18.1	-	0.179(0.078)	0.430(0.137)	1.08	9.17(0.04)	7.47(0.06)	6.23(0.04)	5.11(0.03)	
2381 ^C	G018.218-00.342	18 20 21.94	-13 17 27.4	72.95	0.622(0.095)	3.497(0.372)	3.75	13.55(0.09)	11.06(0.06)	9.85(0.05)	8.92(0.03)	
2431 [*]	G018.666+00.032	18 24 52.00	-12 39 12.6	56.74	0.631(0.065)	2.489(0.233)	3.81	11.96(0.11)	10.46(0.14)	8.13(0.08)	6.47(0.10)	
2439	G018.710+00.001	18 25 04.02	-12 37 46.4	65.53	0.441(0.044)	2.292(0.194)	2.66	10.85(0.10)	9.33(0.08)	7.25(0.06)	5.59(0.07)	
2457	G018.840-00.025	18 25 24.60	-12 31 36.2	-	0.127(0.052)	0.192(0.069)	0.77	12.02(0.13)	10.23(0.09)	9.12(0.05)	8.50(0.04)	
2467 ^{C*}	G018.888-00.475	18 27 08.01	-12 41 38.3	100.92	1.356(0.106)	9.848(0.692)	8.18	12.96(0.08)	10.41(0.20)	9.33(0.07)	9.40(0.12)	
2499 ^{C*}	G019.010-00.029	18 25 44.96	-12 22 41.7	44.10	0.761(0.070)	2.401(0.211)	4.59	11.38(0.12)	7.89(0.08)	6.44(0.03)	6.20(0.03)	
2530	G019.198-00.181	18 26 39.52	-12 16 58.0	-	0.085(0.040)	0.132(0.050)	0.51	13.75(0.10)	11.87(0.10)	10.58(0.09)	9.34(0.07)	
2552	G019.277+00.305	18 25 03.15	-11 59 07.2	37.50	0.224(0.047)	0.753(0.126)	1.35	13.40(0.14)	11.66(0.13)	10.35(0.07)	9.52(0.07)	
2555	G019.288+00.083	18 25 52.47	-12 04 48.4	55.77	0.396(0.049)	1.718(0.172)	2.39	11.65(0.05)	9.69(0.06)	8.98(0.04)	8.38(0.04)	
2576 [*]	G019.488+00.149	18 26 01.03	-11 52 20.7	73.37	0.484(0.054)	3.210(0.249)	2.92	13.72(0.12)	12.42(0.13)	11.03(0.14)	9.73(0.12)	
2579 [*]	G019.498+00.119	18 26 08.68	-11 52 39.2	65.73	0.260(0.037)	1.220(0.137)	1.57	10.96(0.08)	8.93(0.09)	8.19(0.04)	8.35(0.07)	
2619 [*]	G019.756-00.129	18 27 31.95	-11 45 53.1	73.67	0.569(0.051)	2.739(0.229)	3.43	8.80(0.28)	7.34(0.11)	5.47(0.05)	4.24(0.18)	
2630 ^C	G019.827-00.329	18 28 23.57	-11 47 38.3	81.51	0.446(0.047)	2.734(0.240)	2.69	8.97(0.21)	6.71(0.09)	5.33(0.03)	4.63(0.02)	
2636 ^{C*}	G019.884-00.535	18 29 14.68	-11 50 24.0	40.73	2.106(0.147)	5.221(0.394)	12.71	9.25(0.18)	6.75(0.05)	5.45(0.03)	4.87(0.02)	
2641 ^C	G019.926-00.257	18 28 19.10	-11 40 25.5	55.03	0.964(0.073)	3.427(0.263)	5.82	9.22(0.09)	6.93(0.07)	5.25(0.02)	4.10(0.03)	
2649	G019.978-00.213	18 28 15.47	-11 36 26.1	32.49	0.313(0.046)	0.813(0.117)	1.89	11.90(0.05)	10.11(0.06)	8.98(0.04)	8.14(0.06)	
2659 ^{C*}	G020.082-00.135	18 28 10.39	-11 28 44.2	59.03	1.977(0.127)	5.934(0.407)	11.93	11.66(0.10)	9.26(0.17)	7.44(0.05)	5.95(0.06)	
2665 ^{C*}	G020.238+00.065	18 27 44.80	-11 14 52.2	37.39	0.427(0.044)	1.153(0.112)	2.58	11.66(0.10)	8.65(0.08)	7.41(0.03)	7.72(0.03)	
2678	G020.434+00.357	18 27 03.89	-10 56 18.5	20.50	0.139(0.042)	0.296(0.077)	0.84	9.80(0.18)	8.43(0.15)	6.95(0.09)	5.94(0.17)	
2681	G020.440-00.061	18 28 35.06	-11 07 39.2	38.03	0.094(0.032)	0.280(0.069)	0.57	10.94(0.11)	9.27(0.10)	7.88(0.07)	7.24(0.21)	
2696 ^C	G020.545-00.443	18 30 09.87	-11 12 39.2	55.14	0.104(0.035)	0.483(0.095)	0.63	14.30(0.14)	11.92(0.12)	9.97(0.06)	8.99(0.07)	
2697	G020.550+00.059	18 28 21.57	-10 58 27.9	43.31	0.099(0.036)	0.375(0.088)	0.60	11.40(0.08)	9.77(0.07)	8.79(0.05)	8.35(0.06)	
2711 ^C	G020.708-00.311	18 29 59.62	-11 00 22.2	57.17	0.338(0.047)	1.357(0.157)	2.04	14.33(0.14)	11.96(0.09)	10.01(0.06)	8.97(0.06)	
2713 ^C	G020.718-00.359	18 30 11.16	-11 01 10.4	85.71	0.354(0.043)	2.644(0.230)	2.14	12.93(0.10)	10.57(0.06)	9.24(0.04)	8.34(0.03)	
2765	G021.240+00.195	18 29 10.41	-10 18 00.7	38.60	0.372(0.047)	1.086(0.129)	2.25	8.23(0.10)	6.83(0.06)	5.52(0.04)	4.62(0.06)	
2837 ^{C*}	G022.041+00.221	18 30 35.29	-09 34 40.1	87.90	0.953(0.074)	4.676(0.361)	5.75	14.05(0.14)	11.05(0.17)	9.46(0.07)	9.60(0.12)	
2858 ^C	G022.371+00.379	18 30 38.33	-09 12 43.8	65.89	0.409(0.063)	2.409(0.256)	2.47	12.78(0.09)	10.29(0.07)	9.24(0.04)	8.76(0.04)	
2865 ^{C*}	G022.436-00.171	18 32 44.16	-09 24 33.6	53.64	0.444(0.054)	1.596(0.174)	2.68	13.12(0.11)	10.90(0.14)	9.61(0.05)	8.78(0.04)	
2890 ^C	G022.559+00.169	18 31 44.72	-09 08 32.8	51.32	0.270(0.054)	0.928(0.154)	1.63	13.16(0.17)	11.82(0.22)	10.38(0.11)	9.60(0.15)	
2904 ^C	G022.705+00.404	18 31 10.67	-08 54 17.6	74.62	0.279(0.044)	1.755(0.187)	1.68	13.35(0.07)	11.21(0.08)	9.95(0.05)	9.15(0.04)	
2935	G022.836-00.438	18 34 26.81	-09 10 39.9	89.46	0.369(0.055)	2.343(0.244)	2.23	13.60(0.15)	12.15(0.16)	10.63(0.12)	9.65(0.09)	
2994	G023.090-00.394	18 34 45.71	-08 55 55.3	77.73	0.335(0.073)	2.125(0.270)	2.02	11.16(0.14)	9.30(0.10)	7.99(0.05)	7.26(0.09)	
3022 ^C	G023.242-00.482	18 35 21.67	-08 50 15.1	19.07	0.189(0.048)	0.388(0.087)	1.14	11.17(0.08)	9.22(0.10)	7.76(0.04)	6.87(0.03)	
3034 ^C	G023.300-00.074	18 34 00.19	-08 35 54.0	75.90	0.298(0.058)	2.073(0.242)	1.80	12.24(0.11)	10.65(0.10)	9.55(0.05)	9.44(0.04)	
3069	G023.434-00.522	18 35 51.72	-08 41 07.5	33.11	0.192(0.052)	0.467(0.104)	1.16	13.08(0.05)	11.23(0.07)	9.92(0.04)	8.95(0.06)	
3071 ^{C*}	G023.437-00.184	18 34 39.30	-08 31 35.3	118.24	2.146(0.140)	13.906(0.905)	12.95	14.12(0.14)	10.23(0.15)	8.34(0.04)	7.99(0.08)	
3081 ^C	G023.462-00.156	18 34 35.95	-08 29 32.2	58.81	0.349(0.052)	2.034(0.191)	2.11	13.53(0.10)	11.46(0.08)	10.32(0.08)	9.78(0.10)	
3100	G023.520-00.048	18 34 19.16	-08 23 27.9	32.63	0.254(0.042)	0.686(0.097)	1.53	12.01(0.09)	10.38(0.11)	9.17(0.11)	8.34(0.07)	
3131	G023.634+00.038	18 34 13.37	-08 15 01.1	9.89	0.156(0.047)	0.340(0.087)	0.94	13.03(0.07)	11.60(0.08)	10.20(0.06)	9.48(0.06)	
3153 ^{C*}	G023.708-00.198	18 35 12.45	-08 17 35.5	58.05	0.614(0.058)	2.196(0.209)	3.71	13.64(0.11)	12.30(0.14)	10.53(0.14)	9.81(0.14)	
3161	G023.744-00.158	18 35 07.85	-08 14 34.2	-	0.205(0.046)	0.482(0.092)	1.24	12.91(0.10)	10.99(0.07)	10.06(0.10)	9.64(0.08)	
3186 [*]	G023.888+00.060	18 34 36.98	-08 00 52.9	66.35	0.379(0.059)	1.365(0.190)	2.29	12.88(0.08)	11.14(0.12)	9.94(0.06)	9.64(0.08)	
3202 ^{C*}	G023.968-00.110	18 35 22.49	-08 01 18.7	57.34	1.029(0.080)	3.349(0.272)	6.21	14.05(0.23)	10.76(0.10)	9.14(0.05)	9.97(0.08)	
3209 ^C	G024.001+00.250	18 34 08.83	-07 49 33.7	34.41	0.105(0.042)	0.305(0.086)	0.63	14.68(0.17)	12.90(0.18)	11.09(0.14)	9.58(0.09)	
3238	G024.116-00.174	18 35 52.75	-07 55 11.5	77.37	0.488(0.056)	2.478(0.250)	2.95	10.96(0.06)	9.04(0.06)	8.02(0.03)	7.41(0.05)	
3239	G024.119+00.252	18 34 21.56	-07 43 13.3	48.12	0.154(0.053)	0.734(0.139)	0.93	12.56(0.12)	11.08(0.05)	9.71(0.05)	8.98(0.04)	
3258	G024.185+00.120	18 34 57.30	-07 43 21.0	39.55	0.503(0.071)	1.397(0.191)	3.04	10.17(0.17)	8.82(0.07)	7.01(0.12)	5.59(0.10)	
3274 ^C	G024.282-00.008	18 35 35.52	-07 41 46.1	20.57	0.127(0.057)	0.497(0.129)	0.77	9.59(0.19)	7.58(0.04)	6.55(0.04)	5.87(0.02)	
3283	G024.324-00.122	18 36 04.71	-07 42 40.4	51.57	0.231(0.061)	0.939(0.175)	1.39	9.45(0.04)	7.78(0.05)	6.50(0.03)	6.32(0.04)	
3284 ^{C*}	G024.329+00.142	18 35 08.61	-07 35 04.3	42.32	1.564(0.112)	4.381(0.330)	9.44	12.79(0.09)	9.11(0.34)	7.41(0.06)	6.95(0.06)	
3342	G024.498+00.054	18 35 46.45	-07 28 26.5	44.25	0.214(0.061)	0.716(0.154)	1.29	12.52(0.11)	10.53(0.08)	9.56(0.06)	9.41(0.07)	
3354 [*]	G024.541+00.314	18 34 55.25	-07 19 01.8	39.78	0.311(0.058)	0.824(0.134)	1.88	13.34(0.08)	11.70(0.07)	10.22(0.05)	9.50(0.06)	
3369	G024.577-00.074	18 36 22.64	-07 27 48.9	-	0.142(0.049)	0.250(0.076)	0.86	11.66(0.05)	9.75(0.04)	8.66(0.03)	8.10(0.06)	
3380	G024.615+00.421	18 34 40.72	-07 12 09.7	62.34	0.136(0.043)	0.819(0.144)	0.82	11.33(0.08)	9.48(0.03)	8.33(0.04)	7.36(0.02)	

Table B.1. continued.

		BGPS source						GLIMPSE point source			
PID	Name	RA	Dec	R	$S_{40''}$	S_{int}	N_{H_2}	3.6 μm	4.5 μm	5.8 μm	8.0 μm
(1)	(2)	(J2000)	(J2000)	($''$)	(Jy)	(Jy)	10^{22} cm^{-2}	(mag)	(mag)	(mag)	(mag)
(3)	(4)	(5)	(6)	(7)	(8)	(9)	(10)	(11)	(12)	(13)	(14)
3381	G024.628-00.101	18 36 34.22	-07 25 55.3	54.59	0.486(0.067)	2.087(0.231)	2.93	10.31(0.03)	8.48(0.03)	7.36(0.02)	6.79(0.02)
3383 ^C	G024.632+00.155	18 35 39.87	-07 18 32.7	50.03	0.618(0.060)	1.980(0.189)	3.73	11.13(0.06)	8.28(0.07)	7.33(0.03)	6.76(0.03)
3394 ^{C*}	G024.676-00.151	18 36 50.31	-07 24 44.5	68.17	1.658(0.126)	7.278(0.531)	10.01	11.75(0.25)	9.40(0.24)	7.95(0.12)	7.02(0.17)
3402 ^C	G024.728+00.153	18 35 50.97	-07 13 29.1	28.35	0.418(0.061)	1.051(0.142)	2.52	9.43(0.11)	7.18(0.07)	5.64(0.02)	4.79(0.02)
3413 ^{C*}	G024.791+00.083	18 36 12.90	-07 12 06.6	73.40	4.790(0.301)	17.786(1.141)	28.91	11.55(0.12)	7.78(0.05)	6.19(0.02)	6.34(0.05)
3436	G024.916-00.131	18 37 12.67	-07 11 24.0	50.32	0.284(0.065)	1.312(0.189)	1.71	13.30(0.06)	11.53(0.06)	10.68(0.06)	9.65(0.04)
3440 [*]	G024.943+00.075	18 36 31.51	-07 04 13.9	49.32	0.503(0.062)	1.403(0.187)	3.04	13.74(0.16)	12.38(0.32)	10.40(0.09)	9.36(0.10)
3463	G025.158+00.175	18 36 34.03	-06 49 57.8	–	0.192(0.065)	0.465(0.124)	1.16	10.42(0.17)	8.85(0.21)	7.22(0.05)	6.04(0.06)
3466 ^C	G025.179+00.213	18 36 28.09	-06 47 51.0	64.15	0.215(0.056)	1.189(0.185)	1.30	10.92(0.08)	8.63(0.06)	7.28(0.03)	6.60(0.04)
3474	G025.227+00.289	18 36 17.11	-06 43 11.8	44.05	0.769(0.078)	2.290(0.229)	4.64	13.30(0.14)	11.54(0.13)	10.60(0.11)	9.88(0.10)
3504 ^C	G025.394+00.363	18 38 55.53	-06 52 18.1	38.93	0.361(0.054)	1.103(0.145)	2.18	12.55(0.10)	10.44(0.05)	9.24(0.05)	8.61(0.08)
3505 ^{C*}	G025.395+00.033	18 37 30.70	-06 41 17.8	63.10	0.645(0.070)	2.889(0.266)	3.89	9.52(0.16)	7.28(0.10)	5.49(0.05)	4.53(0.08)
3528 ^C	G025.515+00.141	18 37 20.83	-06 31 55.6	–	0.177(0.051)	0.288(0.075)	1.07	14.32(0.26)	11.57(0.08)	10.30(0.07)	9.85(0.09)
3530 ^C	G025.516-00.205	18 38 35.11	-06 41 27.1	32.07	0.164(0.044)	0.454(0.093)	0.99	11.05(0.12)	8.27(0.14)	6.51(0.02)	5.44(0.03)
3548	G025.615-00.137	18 38 31.59	-06 34 14.9	–	0.316(0.067)	0.764(0.134)	1.91	9.13(0.10)	7.52(0.06)	6.12(0.03)	5.15(0.04)
3557	G025.661-00.161	18 38 41.83	-06 32 27.4	29.52	0.206(0.047)	0.595(0.107)	1.24	13.50(0.13)	12.09(0.31)	10.63(0.10)	9.89(0.08)
3560	G025.673-00.043	18 38 17.83	-06 28 34.2	–	0.160(0.077)	0.316(0.120)	0.97	12.19(0.06)	10.33(0.06)	9.08(0.05)	8.60(0.06)
3589	G025.797+00.073	18 38 06.68	-06 18 46.0	22.59	0.249(0.065)	0.559(0.126)	1.50	14.17(0.16)	12.53(0.13)	10.36(0.10)	8.77(0.15)
3591	G025.805-00.041	18 38 32.02	-06 21 28.6	60.60	0.765(0.068)	2.616(0.235)	4.62	13.11(0.09)	11.22(0.14)	10.06(0.08)	9.74(0.12)
3616	G025.920-00.139	18 39 05.90	-06 17 59.3	44.03	0.134(0.055)	0.553(0.127)	0.81	10.12(0.06)	8.37(0.05)	7.38(0.04)	6.82(0.03)
3648	G026.233+00.097	18 38 49.80	-05 54 51.6	8.26	0.162(0.065)	0.390(0.114)	0.98	12.82(0.08)	11.15(0.07)	10.02(0.06)	9.27(0.08)
3670	G026.446-00.031	18 39 40.91	-05 46 58.2	49.35	0.080(0.039)	0.257(0.076)	0.48	11.02(0.13)	9.26(0.04)	8.11(0.03)	7.28(0.02)
3678	G026.507-00.447	18 41 16.76	-05 55 12.0	–	0.118(0.055)	0.180(0.073)	0.71	12.64(0.07)	10.80(0.07)	9.71(0.06)	9.04(0.05)
3679	G026.510+00.281	18 38 41.10	-05 34 58.5	44.64	2.367(0.156)	6.081(0.429)	14.29	12.46(0.12)	10.75(0.09)	8.30(0.05)	6.79(0.11)
3683 [*]	G026.529-00.267	18 40 40.57	-05 49 04.9	43.70	0.296(0.057)	1.063(0.157)	1.79	9.20(0.14)	7.39(0.05)	6.13(0.05)	5.23(0.08)
3690	G026.562-00.303	18 40 52.05	-05 48 15.5	72.07	0.825(0.076)	3.418(0.288)	4.98	12.91(0.14)	11.58(0.13)	10.09(0.21)	8.49(0.15)
3699 ^{C*}	G026.597-00.025	18 39 56.20	-05 38 48.3	46.31	0.509(0.065)	1.682(0.191)	3.07	10.11(0.19)	7.45(0.08)	5.72(0.05)	5.04(0.12)
3721 ^C	G026.843+00.375	18 38 57.67	-05 14 41.2	18.23	0.142(0.045)	0.354(0.083)	0.86	8.77(0.11)	6.83(0.06)	5.59(0.03)	4.87(0.03)
3741 ^C	G027.019+00.201	18 39 54.38	-05 10 05.2	78.78	0.332(0.055)	1.698(0.212)	2.00	11.53(0.14)	8.75(0.09)	7.49(0.04)	7.34(0.03)
3771 ^C	G027.249+00.109	18 40 39.47	-05 00 21.0	38.85	0.208(0.048)	0.662(0.114)	1.26	11.25(0.06)	8.91(0.09)	7.66(0.03)	7.22(0.04)
3803	G027.535+00.212	18 40 48.92	-04 42 17.0	65.81	0.132(0.039)	0.755(0.128)	0.80	12.53(0.07)	10.61(0.35)	9.46(0.06)	8.62(0.09)
3807	G027.562+00.080	18 41 20.26	-04 44 25.0	53.99	0.876(0.069)	3.499(0.265)	5.29	11.55(0.05)	9.63(0.05)	8.13(0.03)	7.28(0.04)
3822 ^C	G027.743+00.170	18 41 20.84	-04 32 20.6	28.96	0.182(0.041)	0.502(0.090)	1.10	14.53(0.14)	11.68(0.10)	10.44(0.06)	9.82(0.06)
3858	G027.937+00.204	18 41 34.94	-04 21 03.7	80.75	0.476(0.050)	3.070(0.244)	2.87	11.04(0.06)	9.39(0.05)	8.30(0.06)	7.87(0.11)
3863 ^C	G027.972-00.422	18 43 52.92	-04 36 19.3	67.50	0.367(0.040)	1.623(0.158)	2.22	14.07(0.18)	10.89(0.06)	9.86(0.06)	9.37(0.07)
3868	G027.997+00.154	18 41 52.25	-04 19 14.0	48.00	0.182(0.042)	0.789(0.123)	1.10	10.97(0.04)	9.17(0.05)	7.80(0.03)	6.82(0.03)
3897 ^{C*}	G028.147-00.006	18 42 43.01	-04 15 37.5	91.07	0.645(0.052)	3.656(0.282)	3.89	11.37(0.28)	8.76(0.07)	7.06(0.03)	5.58(0.04)
3917 ^C	G028.222+00.358	18 41 33.50	-04 01 34.5	58.12	0.135(0.041)	0.664(0.126)	0.81	13.46(0.23)	11.43(0.15)	10.18(0.14)	9.08(0.10)
3929 [*]	G028.305-00.388	18 44 22.16	-04 17 40.4	69.10	0.738(0.061)	3.980(0.294)	4.45	9.13(0.34)	7.31(0.10)	6.26(0.03)	4.79(0.03)
3938 ^C	G028.341+00.140	18 42 33.13	-04 01 16.0	–	0.118(0.040)	0.204(0.061)	0.71	12.32(0.07)	9.66(0.06)	7.66(0.03)	6.51(0.04)
3946 ^C	G028.361+00.054	18 42 53.73	-04 02 33.6	48.70	0.467(0.051)	1.961(0.176)	2.82	12.92(0.06)	10.60(0.06)	9.63(0.05)	9.06(0.05)
3959 ^C	G028.407-00.436	18 44 43.65	-04 13 32.8	43.32	0.157(0.034)	0.644(0.098)	0.95	13.46(0.10)	10.93(0.09)	9.88(0.05)	9.02(0.05)
3985 ^C	G028.504-00.142	18 43 51.51	-04 00 15.3	74.73	0.214(0.033)	1.164(0.142)	1.29	10.52(0.07)	8.24(0.06)	7.20(0.03)	6.34(0.03)
3994 ^{C*}	G028.533+00.128	18 42 56.83	-03 51 21.2	30.30	0.098(0.035)	0.288(0.074)	0.59	9.52(0.05)	7.45(0.04)	5.88(0.02)	4.85(0.02)
4003 ^C	G028.597-00.022	18 43 35.95	-03 52 03.3	79.18	0.263(0.039)	1.693(0.165)	1.59	9.89(0.06)	7.88(0.04)	6.62(0.03)	5.99(0.04)
4020 ^{C*}	G028.701+00.406	18 42 15.86	-03 34 45.5	26.25	0.259(0.042)	0.593(0.093)	1.56	12.28(0.06)	9.87(0.05)	8.56(0.04)	7.96(0.08)
4027	G028.731+00.180	18 43 07.49	-03 39 21.7	–	0.089(0.045)	0.174(0.070)	0.54	12.89(0.09)	11.11(0.08)	9.94(0.07)	9.25(0.07)
4044	G028.803-00.023	18 43 58.61	-03 41 03.8	49.50	0.360(0.050)	1.209(0.154)	2.17	9.73(0.07)	8.37(0.06)	6.93(0.04)	5.87(0.03)
4055 [*]	G028.831-00.255	18 44 51.31	-03 45 55.9	64.87	1.479(0.100)	4.903(0.353)	8.93	12.27(0.13)	10.80(0.16)	7.86(0.06)	6.36(0.09)
4060 [*]	G028.843+00.493	18 42 12.67	-03 24 46.0	35.80	0.368(0.062)	1.227(0.175)	2.22	11.44(0.08)	8.75(0.07)	7.91(0.03)	7.56(0.04)
4072	G028.927+00.019	18 44 03.26	-03 33 17.6	–	0.097(0.042)	0.227(0.070)	0.59	12.46(0.08)	10.73(0.08)	8.77(0.06)	7.40(0.05)
4082 ^C	G028.963-00.597	18 46 18.99	-03 48 15.7	24.03	0.176(0.065)	0.383(0.113)	1.06	10.51(0.04)	8.26(0.04)	6.61(0.03)	5.57(0.04)
4106 ^C	G029.117+00.025	18 44 22.86	-03 22 59.5	65.07	0.289(0.041)	1.286(0.149)	1.74	12.20(0.12)	9.52(0.07)	8.15(0.04)	7.18(0.03)
4121	G029.225+00.023	18 44 35.16	-03 17 17.0	–	0.292(0.054)	0.537(0.095)	1.76	14.53(0.17)	12.78(0.11)	9.89(0.09)	8.31(0.11)
4133 ^C	G029.277-00.131	18 45 13.80	-03 18 43.9	71.35	0.218(0.038)	1.452(0.163)	1.32	9.12(0.10)	7.02(0.08)	5.89(0.03)	5.32(0.03)
4139 ^{C*}	G029.318-00.165	18 45 25.69	-03 17 25.4	21.24	0.156(0.040)	0.338(0.076)	0.94	11.16(0.12)	8.54(0.07)	7.11(0.03)	6.36(0.03)
4152	G029.397-00.095	18 45 19.29	-03 11 20.5	30.94	0.535(0.056)	1.273(0.138)	3.23	11.66(0.06)	9.74(0.06)	8.54(0.04)	7.92(0.07)
4175	G029.557-00.082	18 45 34.23	-03 02 25.3	37.03	0.076(0.025)	0.239(0.056)	0.46	12.61(0.06)	10.98(0.06)	9.47(0.05)	8.58(0.05)
4207	G029.728+00.072	18 45 19.97	-02 49 07.7	–	0.044(0.031)	0.074(0.039)	0.27	12.11(0.07)	10.27(0.06)	8.91(0.03)	8.07(0.03)
4219 ^C	G029.781-00.262	18 46 37.29	-02 55 23.8	45.50	0.224(0.036)	0.910(0.115)	1.35	12.46(0.08)	10.43(0.08)	9.38(0.08)	8.66(0.09)
4221	G029.794+00.052	18 45 31.48	-02 46 09.2	40.49	0.102(0.031)	0.327(0.070)	0.62	12.57(0.11)	10.81(0.16)	9.34(0.09)	8.28(0.20)
4230	G029.841-00.476	18 47 29.63	-02 58 03.3	39.39	0.174(0.025)	0.603(0.073)	1.05	12.19(0.07)	10.49(0.06)	9.34(0.06)	8.42(0.07)
4238	G029.862+00.028	18 45 44.08	-02 43 10.9	63.57	0.387(0.041)	2.090(0.178)	2.34	13.64(0.10)	12.00(0.08)	10.61(0.08)	9.88(0.06)
4284 ^C	G030.010+00.034	18 45 59.25	-02 35 00.7	–	0.127(0.044)	0.304(0.084)	0.77	12.04(0.06)	9.99(0.05)	8.15(0.03)	7.03(0.03)
4304	G030.102+00.074	18 46 00.58	-02 29 06.7	35.27	0.222(0.036)	0.657(0.086)	1.34	12.64(0.12)	11.13(0.10)	8.70(0.06)	7.06(0.06)
4314	G030.169-00.242	18 47 15.57	-02 34 08.3	36.57	0.090(0.031)	0.292(0.073)	0.54	13.34(0.09)	11.76(0.09)	10.56(0.07)	9.73(0.05)

Table B.1. continued.

		BGPS source						GLIMPSE point source			
PID	Name	RA	Dec	R	$S_{40''}$	S_{int}	N_{H_2}	$3.6 \mu\text{m}$	$4.5 \mu\text{m}$	$5.8 \mu\text{m}$	$8.0 \mu\text{m}$
(1)	(2)	(J2000)	(J2000)	($''$)	(Jy)	(Jy)	10^{22} cm^{-2}	(mag)	(mag)	(mag)	(mag)
(3)	(4)	(5)	(6)	(7)	(8)	(9)	(10)	(11)	(12)	(13)	(14)
4321 ^{C*}	G030.215-00.188	18 47 09.08	-02 30 12.3	83.95	0.917(0.070)	5.916(0.407)	5.53	14.20(0.22)	11.35(0.10)	9.50(0.10)	8.69(0.24)
4348*	G030.298-00.206	18 47 22.13	-02 26 12.8	84.32	0.411(0.045)	2.853(0.238)	2.48	10.54(0.13)	9.06(0.09)	7.19(0.09)	5.83(0.11)
4366 ^C	G030.347+00.390	18 45 20.04	-02 07 19.3	77.98	0.387(0.039)	1.973(0.178)	2.34	10.75(0.09)	8.27(0.09)	7.05(0.04)	6.68(0.04)
4384	G030.387-00.106	18 47 10.41	-02 18 46.6	97.62	0.857(0.062)	5.456(0.378)	5.17	10.22(0.09)	8.87(0.07)	7.36(0.08)	6.52(0.23)
4398 ^C	G030.419-00.232	18 47 40.85	-02 20 31.2	87.20	1.500(0.102)	7.704(0.522)	9.05	12.66(0.15)	10.36(0.30)	9.01(0.06)	8.29(0.08)
4403*	G030.423+00.466	18 45 12.15	-02 01 10.9	84.23	0.348(0.041)	2.312(0.212)	2.10	13.67(0.23)	12.06(0.16)	10.19(0.14)	8.68(0.11)
4406	G030.431-00.116	18 47 17.37	-02 16 42.1	63.70	0.306(0.051)	1.770(0.193)	1.85	12.85(0.08)	11.05(0.07)	9.86(0.06)	9.06(0.06)
4407	G030.435-00.380	18 48 14.23	-02 23 43.2	37.16	0.204(0.038)	0.676(0.097)	1.23	8.97(0.09)	7.03(0.15)	5.66(0.04)	5.30(0.04)
4416	G030.463+00.032	18 46 49.26	-02 10 56.4	60.05	0.395(0.041)	1.440(0.145)	2.38	9.56(0.16)	7.62(0.16)	5.95(0.04)	5.10(0.05)
4441	G030.504+00.173	18 46 23.42	-02 04 55.4	34.20	0.173(0.034)	0.480(0.080)	1.04	14.20(0.19)	12.44(0.14)	10.45(0.07)	9.47(0.05)
4472 ^C	G030.603+00.175	18 46 33.95	-01 59 31.8	128.72	1.462(0.098)	12.965(0.830)	8.82	12.43(0.06)	9.07(0.18)	7.14(0.03)	6.93(0.03)
4485	G030.632+00.085	18 46 56.25	-02 00 29.9	49.23	0.133(0.032)	0.598(0.093)	0.80	12.69(0.07)	10.85(0.05)	9.42(0.05)	8.75(0.04)
4487	G030.650-00.119	18 47 41.82	-02 05 07.3	32.50	0.210(0.031)	0.636(0.072)	1.27	12.89(0.05)	11.38(0.06)	10.14(0.06)	9.56(0.08)
4488	G030.652-00.203	18 47 59.99	-02 07 18.9	53.48	0.852(0.063)	2.867(0.213)	5.14	12.22(0.15)	10.56(0.11)	9.34(0.07)	8.64(0.05)
4492 ^C	G030.666-00.139	18 47 47.84	-02 04 48.9	53.89	0.298(0.034)	1.316(0.123)	1.80	13.47(0.13)	11.22(0.09)	9.74(0.11)	9.12(0.17)
4497 ^C	G030.667-00.331	18 48 29.10	-02 09 57.8	-	0.116(0.027)	0.192(0.044)	0.70	9.72(0.18)	7.42(0.08)	6.12(0.02)	4.09(0.03)
4507	G030.699-00.111	18 47 45.58	-02 02 14.0	45.60	0.096(0.036)	0.357(0.086)	0.58	10.77(0.07)	9.42(0.05)	8.15(0.03)	7.37(0.04)
4523 [†]	G030.734-00.297	18 48 29.06	-02 05 30.6	47.82	0.127(0.027)	0.598(0.077)	0.77	10.27(0.10)	8.78(0.09)	7.27(0.05)	6.28(0.09)
4529	G030.754+00.109	18 47 04.49	-01 53 19.7	43.57	0.329(0.050)	1.001(0.120)	1.99	12.72(0.09)	11.37(0.11)	9.05(0.06)	7.51(0.09)
4547*	G030.788+00.205	18 46 47.70	-01 48 53.1	52.84	1.074(0.074)	3.332(0.235)	6.48	11.18(0.09)	9.03(0.15)	8.11(0.08)	7.39(0.05)
4581 ^C	G030.868-00.121	18 48 06.12	-01 53 32.3	73.45	0.420(0.040)	3.184(0.226)	2.53	14.42(0.33)	12.13(0.24)	10.57(0.15)	9.52(0.26)
4594*	G030.896+00.139	18 47 13.64	-01 44 55.6	92.03	0.906(0.072)	6.859(0.460)	5.47	12.69(0.08)	10.77(0.08)	9.58(0.06)	9.15(0.10)
4598*	G030.900+00.163	18 47 08.95	-01 44 03.3	107.93	0.794(0.062)	6.065(0.414)	4.79	12.37(0.05)	10.79(0.08)	8.80(0.03)	7.44(0.03)
4608	G030.922+00.091	18 47 26.74	-01 44 51.1	74.70	0.444(0.036)	2.047(0.162)	2.68	9.77(0.07)	8.40(0.09)	6.99(0.05)	6.17(0.11)
4621 ^C	G030.948+00.159	18 47 15.06	-01 41 36.1	28.30	0.125(0.032)	0.351(0.066)	0.75	11.54(0.07)	9.34(0.05)	8.19(0.03)	7.36(0.03)
4627 ^C	G030.960+00.085	18 47 32.19	-01 42 59.2	54.60	0.600(0.046)	2.191(0.166)	3.62	9.05(0.19)	6.89(0.08)	5.26(0.04)	4.57(0.13)
4633*	G030.974-00.139	18 48 21.58	-01 48 22.3	105.75	0.684(0.052)	5.739(0.394)	4.13	10.33(0.14)	8.34(0.11)	7.35(0.03)	7.17(0.03)
4636	G030.980+00.215	18 47 06.60	-01 38 21.6	90.93	0.474(0.039)	2.594(0.205)	2.86	8.57(0.08)	6.72(0.04)	5.64(0.03)	5.24(0.04)
4642 ^C	G030.998+00.235	18 47 04.30	-01 36 51.1	63.53	0.378(0.037)	2.153(0.163)	2.28	14.15(0.13)	11.55(0.10)	10.43(0.06)	9.89(0.07)
4655	G031.032+00.783	18 45 10.97	-01 20 01.8	38.59	0.178(0.068)	0.649(0.157)	1.07	13.99(0.09)	11.93(0.09)	10.92(0.09)	10.09(0.11)
4670	G031.076-00.105	18 48 25.49	-01 41 59.7	71.78	0.147(0.030)	0.836(0.114)	0.89	13.12(0.09)	11.27(0.08)	10.30(0.07)	9.58(0.08)
4673 ^C	G031.077+00.459	18 46 25.22	-01 26 26.8	66.76	0.417(0.040)	2.136(0.173)	2.52	13.78(0.08)	11.44(0.08)	10.22(0.05)	9.93(0.05)
4677	G031.097+00.111	18 47 41.75	-01 34 54.5	18.99	0.145(0.024)	0.296(0.047)	0.88	12.45(0.07)	10.86(0.09)	9.50(0.07)	8.32(0.08)
4678 ^C	G031.103+00.265	18 47 09.51	-01 30 22.3	64.32	0.184(0.029)	1.178(0.121)	1.11	13.93(0.12)	11.16(0.08)	9.72(0.06)	9.21(0.12)
4695*	G031.160+00.049	18 48 01.79	-01 33 17.7	120.79	0.693(0.057)	6.356(0.445)	4.18	11.56(0.31)	10.14(0.10)	7.80(0.06)	6.26(0.08)
4701 ^C	G031.182-00.145	18 48 45.64	-01 37 25.9	73.20	0.289(0.034)	1.824(0.154)	1.74	13.04(0.09)	10.75(0.07)	9.43(0.05)	8.38(0.05)
4718	G031.238-00.069	18 48 35.54	-01 32 21.7	66.48	0.295(0.036)	2.064(0.175)	1.78	11.46(0.08)	9.77(0.05)	8.70(0.04)	8.07(0.03)
4759 ^C	G031.394+00.207	18 47 53.66	-01 16 28.6	87.18	0.207(0.032)	1.407(0.146)	1.25	12.47(0.10)	10.41(0.13)	8.68(0.05)	7.60(0.07)
4790	G031.498+00.177	18 48 11.46	-01 11 44.7	47.53	0.188(0.027)	0.693(0.082)	1.13	8.61(0.07)	6.85(0.06)	5.78(0.03)	5.34(0.05)
4812 ^{C*}	G031.582+00.077	18 48 42.03	-01 09 59.9	73.18	1.053(0.072)	3.928(0.278)	6.36	13.31(0.14)	11.12(0.09)	9.15(0.05)	7.40(0.04)
4822	G031.596+00.323	18 47 51.01	-01 02 31.0	100.90	0.170(0.026)	1.994(0.165)	1.03	13.98(0.09)	12.31(0.09)	11.09(0.07)	9.98(0.14)
4824	G031.606+00.137	18 48 31.84	-01 07 04.5	64.71	0.122(0.027)	0.829(0.101)	0.74	13.46(0.10)	11.67(0.08)	10.45(0.09)	9.65(0.18)
4892 ^C	G031.900+00.343	18 48 20.04	-00 45 44.3	53.48	0.164(0.028)	0.679(0.088)	0.99	13.03(0.09)	10.85(0.08)	10.39(0.06)	9.90(0.08)
4944	G032.227-00.179	18 50 47.44	-00 42 31.0	46.93	0.050(0.028)	0.219(0.067)	0.30	11.61(0.05)	9.94(0.05)	8.53(0.04)	7.60(0.04)
5008 ^C	G032.605-00.253	18 51 44.64	-00 24 21.7	88.71	0.207(0.027)	1.963(0.163)	1.25	14.51(0.22)	11.69(0.11)	9.66(0.05)	8.77(0.08)
5032 ^C	G032.704-00.059	18 51 14.16	-00 13 42.8	46.07	0.333(0.034)	1.151(0.107)	2.01	12.25(0.23)	9.48(0.14)	8.25(0.06)	7.59(0.12)
5041*	G032.744-00.075	18 51 21.95	-00 12 00.9	50.63	1.174(0.076)	4.008(0.265)	7.09	14.79(0.22)	13.36(0.18)	10.71(0.08)	9.11(0.09)
5050	G032.773-00.059	18 51 21.60	-00 10 04.9	58.16	0.129(0.028)	0.586(0.087)	0.78	10.98(0.12)	9.53(0.11)	8.26(0.04)	7.22(0.03)
5061 ^C	G032.829-00.081	18 51 32.43	-00 07 41.7	71.84	0.227(0.029)	1.147(0.119)	1.37	12.66(0.20)	10.22(0.05)	9.26(0.06)	8.87(0.06)
5091	G032.960-00.339	18 52 41.98	-00 07 42.7	29.73	0.085(0.024)	0.209(0.046)	0.51	11.63(0.18)	9.78(0.30)	8.92(0.12)	8.58(0.21)
5100 ^{C*}	G032.991+00.037	18 51 24.97	+00 04 11.1	75.21	0.759(0.055)	3.401(0.249)	4.58	10.59(0.06)	8.55(0.12)	7.40(0.04)	6.93(0.04)
5116	G033.100+00.069	18 51 29.97	+00 10 49.6	133.78	0.457(0.041)	5.718(0.405)	2.76	10.70(0.05)	9.01(0.06)	8.06(0.03)	7.39(0.04)
5140	G033.265+00.069	18 51 48.15	+00 19 41.3	76.93	0.464(0.039)	2.537(0.195)	2.80	11.99(0.06)	10.12(0.06)	8.90(0.09)	8.26(0.19)
5147	G033.304+00.100	18 51 45.48	+00 22 35.6	-	0.055(0.029)	0.086(0.037)	0.33	12.49(0.07)	11.02(0.06)	9.80(0.06)	8.96(0.05)
5150	G033.314-00.358	18 53 24.60	+00 10 41.5	-	0.114(0.028)	0.235(0.048)	0.69	11.49(0.17)	10.10(0.22)	8.29(0.04)	6.74(0.02)
5167 ^{C*}	G033.390+00.008	18 52 14.76	+00 24 46.3	98.64	0.813(0.063)	6.914(0.471)	4.91	10.69(0.08)	7.62(0.04)	6.55(0.03)	5.95(0.03)
5170 ^C	G033.404+00.370	18 50 58.77	+00 35 19.5	-	0.068(0.026)	0.194(0.048)	0.41	13.50(0.13)	11.38(0.07)	9.86(0.06)	8.69(0.06)
5175	G033.424-00.316	18 53 27.68	+00 17 42.8	39.74	0.084(0.028)	0.295(0.066)	0.51	11.06(0.07)	9.60(0.10)	8.44(0.03)	7.61(0.03)
5217 [†]	G033.608+00.229	18 51 51.32	+00 42 23.2	56.93	0.219(0.034)	0.967(0.115)	1.32	11.22(0.21)	9.33(0.16)	7.80(0.09)	6.31(0.14)
5230 ^{C†}	G033.672+00.201	18 52 04.30	+00 45 02.4	65.65	0.144(0.033)	0.799(0.116)	0.87	14.49(0.14)	12.34(0.11)	10.83(0.07)	9.92(0.05)
5237 [†]	G033.692-00.027	18 52 55.20	+00 39 52.6	-	0.185(0.042)	0.381(0.064)	1.12	13.39(0.10)	11.39(0.06)	9.84(0.05)	8.88(0.06)
5239	G033.701-00.413	18 54 18.55	+00 29 45.1	46.21	0.073(0.028)	0.301(0.070)	0.44	13.59(0.14)	12.07(0.17)	10.43(0.07)	9.99(0.08)
5240 ^C	G033.704+00.285	18 51 49.85	+00 49 02.7	40.95	0.269(0.036)	0.963(0.105)	1.62	14.10(0.12)	11.12(0.09)	10.40(0.05)	9.74(0.06)
5241	G033.710+00.133	18 52 22.99	+00 45 12.7	-	0.076(0.030)	0.131(0.043)	0.46	12.09(0.09)	10.61(0.07)	8.68(0.05)	7.15(0.04)
5243	G033.713+00.255	18 51 57.36	+00 48 45.6	-	0.218(0.035)	0.387(0.062)	1.32	11.00(0.15)	9.50(0.10)	7.97(0.10)	6.05(0.12)
5252 ^{C†}	G033.740-00.017	18 52 58.32	+00 42 42.8	90.78	0.708(0.062)	5.136(0.375)	4.27	13.87(0.19)	11.48(0.12)	9.70(0.04)	8.06(0.02)
5265 ^C	G033.817-00.215	18 53 49.15	+00 41 28.0	29.71	0.152(0.037)	0.430(0.077)	0.92	11.26(0.11)	9.24(0.06)	8.65(0.03)	8.24(0.03)
5270 ^{C*}	G033.850+00.017	18 53 03.08	+00 49 31.1	64.54	0.260(0.032)	1.111(0.121)	1.57	13.54(0.10)	10		

Table B.1. continued.

		BGPS source						GLIMPSE point source			
PID	Name	RA	Dec	R	$S_{40''}$	S_{int}	N_{H_2}	$3.6 \mu\text{m}$	$4.5 \mu\text{m}$	$5.8 \mu\text{m}$	$8.0 \mu\text{m}$
(1)	(2)	(J2000)	(J2000)	($''$)	(Jy)	(Jy)	10^{22} cm^{-2}	(mag)	(mag)	(mag)	(mag)
		(3)	(4)	(5)	(6)	(7)	(8)	(9)	(10)	(11)	(12)
5295	G034.018-00.139	18 53 54.78	+00 54 13.5	30.28	0.095(0.035)	0.237(0.064)	0.57	11.61(0.07)	9.91(0.05)	8.54(0.04)	7.55(0.03)
5329	G034.207+00.008	18 53 44.37	+01 08 21.8	80.50	0.207(0.037)	1.190(0.149)	1.25	12.35(0.05)	10.66(0.08)	9.44(0.06)	8.68(0.22)
5342	G034.264-00.210	18 54 37.08	+01 05 23.6	56.55	0.262(0.037)	1.033(0.116)	1.58	13.50(0.12)	12.11(0.10)	10.78(0.09)	10.07(0.06)
5344	G034.276-00.152	18 54 26.00	+01 07 37.2	41.46	0.238(0.036)	0.756(0.098)	1.44	11.48(0.19)	9.85(0.10)	7.53(0.10)	6.01(0.12)
5373 ^{C*}	G034.410+00.232	18 53 18.61	+01 25 16.6	96.10	3.337(0.210)	20.777(1.303)	20.14	14.15(0.20)	11.36(0.17)	10.55(0.12)	10.02(0.12)
5414	G034.591+00.244	18 53 35.95	+01 35 19.5	73.12	0.224(0.031)	1.114(0.123)	1.35	12.98(0.06)	11.02(0.05)	9.44(0.05)	8.52(0.06)
5421	G034.624-00.132	18 54 59.80	+01 26 45.0	73.85	0.216(0.033)	1.282(0.141)	1.30	8.68(0.28)	7.18(0.09)	5.78(0.10)	4.84(0.15)
5426	G034.677-00.110	18 55 01.01	+01 30 14.1	–	0.110(0.038)	0.226(0.062)	0.66	12.72(0.08)	10.90(0.07)	9.51(0.05)	8.63(0.13)
5474	G034.846+00.060	18 54 43.07	+01 43 51.4	40.63	0.144(0.035)	0.472(0.084)	0.87	11.00(0.10)	9.39(0.06)	8.32(0.04)	7.22(0.04)
5499	G034.922+00.136	18 54 35.15	+01 49 59.7	61.21	0.137(0.032)	0.787(0.107)	0.83	13.05(0.09)	11.12(0.14)	10.41(0.10)	9.84(0.13)
5501 ^C	G034.932+00.022	18 55 00.61	+01 47 24.6	71.21	0.254(0.037)	1.292(0.147)	1.53	13.99(0.19)	11.76(0.08)	9.25(0.04)	7.79(0.04)
5516 ^{C†}	G034.991-00.046	18 55 21.71	+01 48 45.2	46.34	0.163(0.037)	0.689(0.104)	0.98	12.11(0.09)	9.62(0.10)	8.46(0.04)	7.77(0.04)
5572 ^{C†}	G035.228-00.358	18 56 54.23	+01 52 48.9	22.89	0.364(0.043)	0.784(0.095)	2.20	11.47(0.06)	9.33(0.05)	8.04(0.04)	7.10(0.03)
5577 ^{C*}	G035.247-00.238	18 56 30.78	+01 57 10.0	–	0.087(0.038)	0.123(0.047)	0.53	11.77(0.19)	9.37(0.10)	8.74(0.04)	7.78(0.03)
5594 ^{C†}	G035.316-00.222	18 56 34.81	+02 01 14.1	58.23	0.149(0.036)	0.673(0.111)	0.90	12.16(0.12)	10.10(0.09)	9.15(0.04)	8.12(0.03)
5626 [†]	G035.457-00.180	18 56 41.39	+02 09 58.0	74.31	0.327(0.039)	1.466(0.156)	1.97	13.82(0.14)	11.81(0.24)	9.65(0.08)	8.11(0.10)
5633 [†]	G035.481+00.224	18 55 17.67	+02 22 18.3	18.08	0.142(0.035)	0.277(0.058)	0.86	12.65(0.13)	11.35(0.09)	9.32(0.08)	7.76(0.15)
5639 [†]	G035.497-00.018	18 56 11.15	+02 16 32.2	105.07	0.454(0.051)	4.138(0.330)	2.74	10.65(0.07)	8.67(0.05)	7.61(0.04)	6.95(0.04)
5691 ^{C†}	G035.707+00.164	18 55 55.25	+02 32 43.8	–	0.065(0.032)	0.084(0.036)	0.39	12.84(0.13)	10.49(0.07)	9.39(0.04)	8.82(0.04)
5720 ^C	G035.997-00.466	18 58 41.71	+02 30 57.5	79.56	0.163(0.034)	1.266(0.146)	0.98	13.50(0.13)	11.43(0.08)	10.00(0.05)	8.99(0.03)
5757	G036.411+00.122	18 57 21.43	+03 09 09.9	78.29	0.100(0.028)	0.728(0.107)	0.60	9.36(0.10)	7.86(0.05)	6.63(0.03)	5.81(0.03)
5782 ^{C*}	G036.704+00.094	18 57 59.47	+03 23 59.0	70.92	0.156(0.037)	1.088(0.147)	0.94	10.75(0.08)	8.69(0.07)	8.09(0.04)	7.70(0.03)
5788	G036.768-00.088	18 58 45.42	+03 22 24.7	25.19	0.055(0.035)	0.148(0.058)	0.33	11.48(0.05)	9.67(0.06)	8.68(0.04)	8.07(0.03)
5802	G036.880-00.474	19 00 20.27	+03 17 48.1	39.50	0.251(0.038)	0.764(0.102)	1.51	8.35(0.09)	7.02(0.10)	5.74(0.04)	5.05(0.09)
5807*	G036.920+00.484	18 56 59.75	+03 46 11.9	19.48	0.186(0.055)	0.373(0.096)	1.12	10.04(0.09)	8.34(0.04)	7.00(0.04)	5.91(0.08)
5821	G037.201-00.418	19 00 43.70	+03 36 31.1	31.22	0.269(0.045)	0.695(0.109)	1.62	11.11(0.10)	9.14(0.13)	7.90(0.05)	6.87(0.03)
5836 ^C	G037.341-00.062	18 59 42.95	+03 53 45.3	79.89	0.445(0.045)	2.281(0.204)	2.69	9.93(0.11)	7.62(0.08)	5.75(0.03)	4.68(0.05)
5847*	G037.475-00.102	19 00 06.25	+03 59 48.5	36.95	0.303(0.058)	0.834(0.135)	1.83	12.64(0.15)	10.81(0.11)	9.40(0.06)	9.30(0.08)
5894*	G038.119-00.232	19 01 44.86	+04 30 33.9	21.37	0.266(0.047)	0.699(0.108)	1.61	9.26(0.13)	7.47(0.07)	6.40(0.03)	5.72(0.08)
5896 ^C	G038.161-00.078	19 01 16.50	+04 37 01.8	33.10	0.151(0.049)	0.426(0.102)	0.91	13.82(0.08)	11.79(0.09)	10.44(0.07)	9.98(0.11)
5898	G038.195-00.156	19 01 36.95	+04 36 42.3	53.35	0.198(0.046)	0.740(0.125)	1.20	10.06(0.09)	8.68(0.05)	7.24(0.03)	6.12(0.05)
5901*	G038.256-00.076	19 01 26.64	+04 42 12.4	–	0.146(0.043)	0.339(0.082)	0.88	10.74(0.05)	8.82(0.05)	7.45(0.03)	6.12(0.02)
5934	G038.730-00.510	19 03 51.60	+04 55 28.1	35.64	0.131(0.040)	0.411(0.090)	0.79	11.97(0.05)	10.50(0.05)	9.11(0.03)	7.75(0.02)
5941 ^C	G038.847-00.428	19 03 47.06	+05 04 00.9	85.04	0.246(0.037)	1.435(0.159)	1.48	13.18(0.06)	10.88(0.06)	9.65(0.05)	8.66(0.05)
5949 [†]	G038.872-00.182	19 02 57.23	+05 12 09.7	–	0.082(0.037)	0.146(0.054)	0.49	13.01(0.07)	11.52(0.08)	10.32(0.08)	9.96(0.05)
5957	G038.920-00.418	19 03 53.09	+05 08 14.2	58.81	0.220(0.042)	1.190(0.148)	1.33	13.37(0.16)	11.86(0.11)	10.34(0.12)	9.74(0.17)
5970	G039.197+00.223	19 02 06.38	+05 40 32.3	25.00	0.174(0.037)	0.407(0.074)	1.05	10.67(0.10)	9.16(0.11)	7.61(0.04)	5.88(0.07)
5993 ^C	G039.591-00.205	19 04 21.68	+05 49 47.5	60.24	0.190(0.043)	1.069(0.149)	1.15	13.33(0.08)	11.27(0.06)	10.26(0.05)	9.76(0.10)
6017 ^C	G040.157+00.167	19 04 04.51	+06 30 12.3	–	0.111(0.039)	0.220(0.063)	0.67	8.71(0.15)	7.41(0.14)	6.04(0.05)	4.90(0.10)
6022	G040.265-00.467	19 06 32.51	+06 18 30.2	20.99	0.132(0.045)	0.292(0.082)	0.80	12.73(0.09)	11.13(0.09)	10.08(0.05)	9.40(0.05)
6023 ^C	G040.279-00.269	19 05 51.60	+06 24 42.4	31.00	0.187(0.044)	0.458(0.092)	1.13	10.58(0.13)	8.43(0.09)	7.35(0.03)	6.69(0.03)
6026	G040.361-00.061	19 05 16.05	+06 34 48.4	13.71	0.102(0.045)	0.203(0.070)	0.62	13.22(0.06)	11.64(0.08)	10.61(0.06)	9.88(0.06)
6029*	G040.622-00.139	19 06 01.86	+06 46 37.3	56.05	0.834(0.067)	2.961(0.244)	5.03	14.92(0.29)	13.42(0.23)	10.02(0.14)	8.37(0.30)
6086 ^C	G041.883+00.469	19 06 11.27	+08 10 31.7	–	0.116(0.047)	0.265(0.081)	0.70	14.57(0.23)	12.46(0.11)	10.39(0.06)	9.08(0.06)
6096	G042.099+00.351	19 07 00.77	+08 18 47.0	42.56	0.282(0.045)	0.862(0.122)	1.70	9.07(0.22)	7.10(0.09)	5.34(0.03)	4.30(0.04)
6110 ^{C*}	G043.039-00.455	19 11 39.57	+08 46 30.4	27.60	0.794(0.074)	1.706(0.168)	4.79	13.10(0.09)	10.89(0.09)	9.95(0.07)	9.13(0.06)
6111 ^{C*}	G043.073-00.079	19 10 22.40	+08 58 44.8	31.59	0.237(0.061)	0.614(0.128)	1.43	12.21(0.05)	10.59(0.05)	9.56(0.04)	8.90(0.04)
6131 ^C	G043.929-00.335	19 12 53.93	+09 37 11.3	14.35	0.114(0.043)	0.231(0.071)	0.69	13.46(0.12)	10.92(0.10)	9.78(0.06)	8.85(0.05)
6137 ^C	G044.099+00.163	19 11 25.56	+10 00 03.4	20.12	0.141(0.048)	0.377(0.093)	0.85	11.97(0.07)	9.70(0.06)	8.60(0.04)	7.82(0.03)
6153 ^C	G044.521+00.387	19 11 24.68	+10 28 43.3	23.84	0.221(0.049)	0.551(0.101)	1.33	10.69(0.07)	9.10(0.06)	7.60(0.03)	6.39(0.04)
6166 ^C	G045.167+00.095	19 13 40.95	+10 54 57.8	39.35	0.189(0.053)	0.654(0.127)	1.14	11.89(0.15)	9.28(0.07)	7.81(0.04)	6.64(0.03)
6208 ^C	G045.884-00.509	19 17 13.41	+11 16 14.0	–	0.196(0.050)	0.480(0.093)	1.18	11.69(0.06)	9.73(0.05)	8.69(0.04)	7.86(0.03)
6225 ^C	G046.314-00.213	19 16 58.42	+11 47 20.2	30.28	0.129(0.039)	0.407(0.085)	0.78	13.00(0.08)	11.04(0.07)	9.99(0.07)	9.53(0.07)
6258 ^C	G048.609+00.220	19 19 48.70	+14 01 11.2	–	0.126(0.057)	0.240(0.081)	0.76	12.01(0.07)	10.06(0.05)	8.91(0.05)	8.16(0.04)
6280 ^C	G048.841-00.482	19 22 48.67	+13 53 34.3	59.75	0.203(0.055)	0.833(0.158)	1.23	13.88(0.07)	12.21(0.10)	11.04(0.10)	10.06(0.07)
6298 ^C	G049.069-00.328	19 22 41.65	+14 09 59.4	63.88	0.660(0.079)	3.313(0.317)	3.98	10.22(0.14)	8.31(0.09)	6.91(0.03)	6.08(0.03)
6304 ^C	G049.106-00.272	19 22 33.86	+14 13 35.1	28.96	0.189(0.054)	0.625(0.108)	1.14	13.31(0.22)	11.82(0.08)	10.63(0.14)	10.09(0.20)
6323 ^C	G049.267-00.338	19 23 06.95	+14 20 11.0	51.77	1.662(0.120)	6.088(0.437)	10.03	12.40(0.06)	10.29(0.09)	9.28(0.06)	8.51(0.06)
6338 ^C	G049.378-00.184	19 22 46.39	+14 30 28.0	28.03	0.212(0.051)	0.478(0.101)	1.28	12.26(0.09)	10.59(0.12)	9.28(0.05)	8.33(0.04)
6346 ^C	G049.405-00.370	19 23 30.08	+14 26 34.6	54.92	0.729(0.117)	3.622(0.401)	4.40	12.14(0.11)	9.69(0.07)	7.97(0.05)	6.92(0.07)
6376 ^{C*}	G049.599-00.250	19 23 26.56	+14 40 14.1	24.03	0.362(0.062)	0.862(0.134)	2.18	13.59(0.09)	11.94(0.10)	9.35(0.06)	7.74(0.10)
6380 ^C	G049.817+00.456	19 21 17.62	+15 11 50.1	–	0.109(0.061)	0.226(0.091)	0.66	14.05(0.13)	11.80(0.07)	10.74(0.08)	10.07(0.07)
6387 ^C	G050.060+00.062	19 23 12.41	+15 13 30.5	64.17	0.359(0.071)	2.279(0.265)	2.17	13.24(0.06)	11.38(0.07)	9.98(0.06)	9.22(0.06)
6414 ^{C*}	G053.142+00.068	19 29 18.22	+17 56 19.0	58.07	1.477(0.118)	5.605(0.445)	8.91	8.88(0.20)	7.49(0.16)	6.19(0.05)	4.97(0.04)
6416 ^C	G053.164-00.246	19 30 30.35	+17 48 26.1	38.57	0.468(0.066)	1.272(0.171)	2.82	13.40(0.11)	10.29(0.07)	8.65(0.06)	8.17(0.17)
6424 ^C	G053.248-00.086	19 30 05.13	+17 57 28.0	–	0.127(0.057)	0.288(0.096)	0.77	12.13(0.06)	9.86(0.05)	8.74(0.03)	7.86(0.04)
6429 ^C	G053.457+00.004	19 30 10.65	+18 11 06.7	36.56	0.155(0.069)	0.516(0.147)	0.94	13.58(0.12)	12.27(0.15)	10.92(0.16)	9.38(0.15)

Table B.1. continued.

		BGPS source						GLIMPSE point source			
PID	Name	RA	Dec	R	$S_{40''}$	S_{int}	N_{H_2}	3.6 μm	4.5 μm	5.8 μm	8.0 μm
(1)	(2)	(J2000)	(J2000)	($''$)	(Jy)	(Jy)	10^{22} cm^{-2}	(mag)	(mag)	(mag)	(mag)
(1)	(2)	(3)	(4)	(5)	(6)	(7)	(8)	(9)	(10)	(11)	(12)
6433 ^{C*}	G053.616+00.036	19 30 22.74	+18 20 20.9	41.16	0.618(0.086)	1.894(0.239)	3.73	10.01(0.21)	7.39(0.16)	5.69(0.03)	4.94(0.03)
6445 ^C	G053.942-00.080	19 31 28.15	+18 34 08.9	19.49	0.091(0.060)	0.264(0.102)	0.55	10.88(0.05)	9.26(0.04)	8.03(0.03)	7.16(0.04)
6451 ^C	G054.112-00.083	19 31 49.34	+18 43 01.6	113.32	0.712(0.097)	6.994(0.586)	4.30	9.26(0.07)	7.90(0.07)	6.58(0.03)	5.57(0.03)
6455 ^C	G054.390-00.035	19 32 12.69	+18 59 01.5	31.23	0.225(0.070)	0.664(0.149)	1.36	10.15(0.09)	8.61(0.05)	7.35(0.02)	6.43(0.04)
6470 ^C	G056.962-00.234	19 38 16.80	+21 08 02.2	25.81	0.243(0.090)	0.630(0.170)	1.47	9.49(0.17)	7.69(0.09)	6.64(0.04)	6.08(0.10)
6474 ^C	G058.471+00.433	19 38 58.22	+22 46 34.6	22.51	0.400(0.000)	0.914(0.212)	2.41	11.16(0.05)	9.53(0.05)	8.40(0.04)	7.67(0.03)
6476 ^C	G059.499-00.235	19 43 42.32	+23 20 20.3	42.20	0.399(0.076)	1.374(0.202)	2.41	10.97(0.07)	8.48(0.06)	6.84(0.03)	5.57(0.03)
6479 ^{C*}	G059.639-00.189	19 43 50.15	+23 28 59.7	39.85	1.531(0.130)	4.660(0.391)	9.24	11.48(0.11)	9.57(0.11)	8.79(0.06)	8.33(0.08)
6492 ^C	G060.017+00.115	19 43 30.46	+23 57 44.9	27.06	0.407(0.088)	1.010(0.172)	2.46	12.58(0.13)	10.42(0.14)	9.49(0.06)	8.23(0.08)
6501 ^C	G063.075+00.184	19 50 03.19	+26 38 23.3	–	0.185(0.080)	0.200(0.102)	1.12	11.63(0.14)	9.41(0.07)	8.13(0.04)	6.91(0.03)

Table B.2. Related parameters of the class II methanol masers from the literature.

PID	Maser	Offset	Distance	6.7 GHz CH ₃ OH							BGPS source		
				V_{start}	V_{end}	V_p	S_p	S_{int}	Luminosity	ref.	M	$n(\text{H}_2)$	$N(\text{H}_2)$
(1)	(2)	($''$)	(kpc)	km s^{-1}	km s^{-1}	km s^{-1}	(Jy)	(Jy km s^{-1})	($10^{-7} L_{\odot}$)	(11)	(M_{\odot})	(10^3 cm^{-3})	(10^{22} cm^{-2})
1031	04.569-0.079	0	2.8 ^N	9.0	10.0	9.5	0.4	–	–	1	102	0.8	0.3
1144	05.900-0.430	111	1.6 ^G	0.0	10.6	10.4	6.2	–	–	1	16	–	–
1175	06.189-0.358	7	5.1 ^G	–37.5	–27.1	–30.2	228.6	–	–	2, 0	2420	5.8	2.8
1240	06.795-0.257	15	3.0 ^N	12.1	31.4	16.3	91.1	–	–	2	818	15.4	3.8
1352	08.317-0.096	30	11.7 ^G	44.6	48.7	46.9	2.0	2.7	115.6	3	958	–	–
1395	08.832-0.028	0	5.2 ^G	–6.3	5.7	–3.9	125.8	308.1	2604.7	3	2096	1.5	1.1
1412	09.215-0.202	10	4.4 ^D	36.0	50.0	45.5	12.0	–	–	2	1786	2.8	1.6
1421	09.619+0.193	5	5.2 ^G	5.0	7.0	5.5	70.0	–	–	2	5286	13.0	6.3
1466	10.205-0.345	82	1.6 ^S	5.6	11.0	6.6	2.0	–	–	2	448	6.0	1.7
1479	10.320-0.259	2	3.8 ^S	35.2	40.7	39.0	8.0	10.8	47.5	3	948	2.7	1.2
1497	10.472+0.027	6	11.2 ^G	57.7	78.5	75.0	35.7	108.3	4247.3	3	52302	25.1	21.0
1508	10.627-0.384	4	4.0 ^C	–6.0	7.6	4.5	4.1	7.0	35.0	3	6427	116.1	29.1
1543	10.822-0.103	10	5.4 ^S	68.0	74.0	72.0	0.3	–	–	2	104	–	–
1559	10.958+0.022	9	13.5 ^G	23.5	25.3	24.5	13.4	10.6	604.0	3	9880	1.2	1.6
1592	11.109-0.114	66	13.2 ^G	22.8	34.2	23.9	6.9	11.2	610.1	3	9348	0.4	0.8
1657	11.936-0.150	23	12.2 ^G	46.0	50.0	48.5	2.2	–	–	2	5065	1.7	1.6
1682	12.199-0.033	7	12.0 ^G	48.2	57.1	49.3	13.7	–	–	2, 0	5963	0.8	1.1
1742	12.625-0.017	9	2.7 ^G	20.9	28.0	21.5	14.2	15.6	35.6	3	834	3.1	1.3
1747	12.681-0.182	2	4.7 ^S	50.2	61.6	58.3	306.0	717.9	4901.3	3	5179	2.8	2.3
1803	12.889+0.489	3	2.3 ^G	26.8	40.2	39.2	72.0	90.1	149.0	3	838	16.3	4.0
1809	12.904-0.031	4	4.6 ^S	55.8	61.0	59.1	20.0	–	–	2, 0	1509	2.0	1.2
1865	13.179+0.061	4	4.1 ^G	46.0	49.5	46.4	0.7	0.6	3.2	3	1727	4.5	2.2
2016	14.230-0.509	16	2.2 ^S	24.6	26.7	25.3	0.2	–	–	2	922	9.6	2.9
2081	14.631-0.577	11	13.7 ^G	23.9	25.9	25.2	1.1	–	–	2	38375	1.4	2.8
2246	16.112-0.303	12	3.0 ^G	33.4	35.6	34.5	2.0	–	–	2, 0	69	1.6	0.4
2292	16.585-0.051	3	4.3 ^G	56.4	69.2	62.1	30.8	39.5	228.3	3	1270	17.9	4.9
2330	17.029-0.071	2	10.8 ^G	90.6	94.1	91.3	0.7	0.8	29.2	3	2331	1.4	1.1
2431	18.661+0.034	16	11.2 ^G	76.0	83.0	79.0	8.9	–	–	2	6264	0.9	1.1
2467	18.888-0.475	3	3.8 ^G	53.0	57.6	56.5	5.7	–	–	2, 0	2853	1.8	1.4
2499	19.009-0.029	5	12.0 ^G	53.4	60.8	55.2	9.1	13.6	612.3	3	6937	1.7	1.8
2576	19.486+0.151	9	1.8 ^G	19.0	27.5	20.6	6.0	–	–	2	208	3.2	0.9
2579	19.496+0.115	14	9.8 ^G	120.0	122.0	121.2	7.6	–	–	2, 0	2350	0.3	0.4
2619	19.755-0.128	4	9.9 ^G	115.5	124.0	123.1	3.6	–	–	2, 0	5386	0.5	0.7
2636	19.884-0.534	4	3.3 ^G	46.1	47.9	46.7	9.0	4.6	15.7	3	1140	16.8	4.5
2659	20.085-0.133	13	12.8 ^D	42.3	44.0	43.3	2.2	1.0	51.2	3	19507	1.6	2.4

Notes. Column (1): PID number of BGPS source, all new detections in this survey are marked *, detections that might be a side-lobe of a nearby stronger maser are marked <. Column (2): Galactic coordinates of the associated masers. Column (3): angular offset between the peak of the 1.1 mm dust emission and the maser position. Column (4): adopted distance for sources overlapped with Green & McClure-Griffiths (2011); Dunham et al. (2011), or Schlingman et al. (2011), we preferentially adopted the distances estimated from their work, which are marked by *G*, *D* and *S*, otherwise we adopted the near kinematic distances that computed from the peak velocity of the 6.7 GHz masers, which are marked by *N*. For source PID 1508, the distance cannot be reliably derived from the Galactic rotation curve; we adopted the distance determined by C2012 (marked *C*). Columns (5)–(10): radial velocity range, the radial velocity of the peak emission, peak flux density, integrated flux density, and luminosity of the 6.7 GHz methanol maser. Column (11): references for maser information. 0 This survey. 1 Caswell et al. (2010). 2 Green et al. (2010). 3 Szymczak et al. (2012). Columns (12)–(14): derived gas mass and averaged H₂ volume and column densities of the BGPS source, respectively.

Table B.2. continued.

PID	Maser	Offset (")	Distance (kpc)	6.7 GHz CH ₃ OH							BGPS source		
				V_{start} km s ⁻¹	V_{end} km s ⁻¹	V_p km s ⁻¹	S_p (Jy)	S_{int} (Jy km s ⁻¹)	Luminosity (10 ⁻⁷ L _⊙)	ref.	M (M _⊙)	$n(\text{H}_2)$ (10 ³ cm ⁻³)	$N(\text{H}_2)$ (10 ²² cm ⁻²)
(1)	(2)	(3)	(4)	(5)	(6)	(7)	(8)	(9)	(10)	(11)	(12)	(13)	(14)
2665	20.237+0.065	3	4.4 ^G	68.0	77.8	71.7	49.2	41.0	248.2	3	447	3.6	1.2
2837	22.039+0.222	11	3.3 ^G	45.2	54.8	53.2	4.7	10.5	35.7	3	1021	1.5	0.9
2865	22.435-0.169	5	13.4 ^D	22.1	40.2	29.5	12.3	26.5	1487.7	3	5750	0.6	0.8
3071	23.437-0.184	3	5.9 ^G	101.0	108.0	102.9	69.5	78.4	853.2	3	9708	1.0	1.4
3153	23.707-0.198	4	11.0 ^G	72.6	82.7	76.4	18.4	49.4	1868.8	3	5331	0.7	0.9
3186	23.90+0.06	42	12.4 ^G	35.2	45.3	44.9	1.1	1.2	57.7	3	4211	0.3	0.4
3202	23.966-0.109	5	11.4 ^G	64.0	72.6	70.8	17.1	12.1	491.6	3	8733	1.1	1.5
3284	24.329+0.144	6	9.5 ^G	109.2	120.2	110.3	4.8	8.6	242.7	3	7933	4.4	3.5
3354	24.541+0.312	8	5.5 ^G	104.0	110.3	105.5	12.5	22.9	216.6	3	500	1.7	0.7
3394	24.68-0.16	16	5.9 ^S	111.1	116.9	116.0	4.7	5.6	61.5	3	5131	2.8	2.2
3413	24.790+0.083	6	9.6 ^G	102.1	116.7	113.3	93.5	134.5	3875.4	3	32878	3.4	4.7
3440	24.943+0.074	2	3.0 ^G	45.1	53.7	53.2	4.8	5.3	14.9	3	253	2.8	0.8
3505	25.39+0.03	6	1.1 ^S	94.1	97.5	95.4	0.8	1.2	0.5	3	73	7.3	1.0
3683	26.53-0.27	9	5.2 ^N	102.0	115.3	104.2	5.5	9.4	80.4	3	583	1.7	0.8
3699	26.598-0.024	5	1.6 ^G	17.8	26.4	24.8	8.8	9.5	7.6	3	86	7.6	1.1
3897	28.146-0.005	6	5.3 ^G	97.2	104.9	101.1	28.8	20.3	178.3	3	2060	0.7	0.6
3929	28.305-0.388	2	10.4 ^G	79.6	94.1	81.8	33.7	43.2	1460.8	3	8637	0.8	1.2
3994	28.53+0.13	4	1.7 ^G	23.8	40.0	39.6	1.3	1.7	1.5	3	16	4.4	0.4
4020	28.70+0.40	8	4.8 ^N	92.7	94.5	94.1	1.3	0.7	5.1	3	278	4.9	1.2
4055	28.832-0.253	8	4.6 ^G	79.4	92.7	91.8	55.2	98.0	648.3	3	2081	2.8	1.7
4060	28.84+0.49	2	4.6 ^G	79.8	89.1	83.3	2.0	3.6	23.8	3	520	4.2	1.4
4139	29.32-0.16	12	11.9 ^G	39.9	49.5	48.8	2.0	3.0	132.8	3	960	2.1	1.1
4321	30.225-0.180	46	5.8 ^G	102.6	114.5	113.2	10.6	26.8	281.9	3	3993	1.2	1.2
4348	30.30-0.20	13	5.8 ^S	110.8	114.3	113.1	1.0	1.3	13.5	3	1897	0.6	0.6
4403	30.42+0.46	9	1.3 ^S	5.3	13.7	7.4	1.2	1.5	0.8	3,0	76	2.2	0.5
4547	30.790+0.205	9	9.9 ^G	84.2	90.0	84.5	8.4	20.1	615.9	3	6552	1.6	1.7
4594	30.899+0.162	82	5.6 ^G	98.4	111.7	101.8	55.0	98.6	966.7	3	4315	1.1	1.2
4598	30.899+0.162	6	5.6 ^G	98.4	111.7	101.8	55.0	98.6	966.7	3	3816	0.6	0.7
4633	30.97-0.14	10	4.2 ^G	73.6	80.3	77.8	17.9	25.9	142.8	3	2031	0.8	0.7
4695	31.156+0.045	19	2.6 ^S	40.2	48.2	40.8	2.0	2.0	4.3	3	880	1.0	0.6
4812	31.581+0.077	2	5.2 ^G	95.0	100.3	98.8	4.8	6.7	56.6	3	2131	1.4	1.0
5041	32.745-0.076	1	12.0 ^G	28.0	39.4	38.4	46.4	80.6	3628.7	3	11580	1.8	2.2
5100	32.992+0.034	9	9.1 ^G	89.5	92.7	91.9	9.7	9.8	253.7	3	5651	0.6	0.9
5167	33.39+0.03	71	8.3 ^G	96.6	107.8	105.2	17.6	36.0	775.4	3	9557	0.6	1.0
5270	33.85+0.02	6	10.3 ^G	59.7	64.7	63.9	4.7	4.6	152.6	3	2364	0.3	0.4
5373	34.394+0.221	71	3.4 ^G	55.2	63.1	55.6	22.1	16.5	59.6	3	4817	4.9	3.2
5577	35.247-0.237	5	4.1 ^G	71.2	73.0	72.4	1.6	0.9	4.7	3	41	–	–
5782	36.705+0.096	8	10.2 ^G	52.3	62.6	53.0	5.0	5.7	185.4	3	2271	0.2	0.3
5807	36.918+0.483	8	16.7 ^G	-36.3	-35.5	-35.8	1.2	0.8	69.8	3	2087	2.2	1.4
5847	37.479-0.105	14	3.5 ^G	53.6	63.2	54.7	8.5	27.9	106.9	3	204	3.4	0.9
5894	38.119-0.229	11	4.3 ^G	66.5	79.7	70.4	2.6	5.6	32.4	3	259	11.9	2.2
5901	38.258-0.073	9	0.8 ^G	6.2	15.7	15.4	8.0	4.8	1.0	3	4	–	–
6029	40.623-0.138	3	1.9 ^G	29.6	36.5	31.1	12.9	6.3	7.1	3	214	6.3	1.3
6110	43.038-0.453	8	3.5 ^G	54.1	63.2	54.8	5.3	6.6	25.3	3	419	16.6	3.2
6111	43.074-0.077	8	11.7 ^G	9.6	11.2	10.2	8.7	3.8	162.6	3	1686	1.2	0.9
6376	49.599-0.249	2	5.4 ^G	57.3	67.0	63.0	41.8	86.7	790.4	3	504	8.3	2.1
6414	53.142+0.071	10	1.6 ^G	23.4	25.4	24.6	2.6	1.2	1.0	3,0	287	12.8	2.4
6433	53.618+0.036	6	8.7 ^G	18.1	19.7	18.9	7.9	3.9	92.3	3,0	2876	2.2	1.6
6479	59.63-0.19	23	3.5 ^S	29.1	30.5	29.5	3.3	1.5	5.7	3,0	1132	15.2	4.2